Sedimentary Geology 372 (2018) 1–24

Contents lists available at ScienceDirect

Sedimentary Geology

journal homepage: www.elsevier.com/locate/sedgeo

Palaeoredox conditions and sequence stratigraphy of the Cretaceous storm-dominated, mixed siliciclastic-carbonate ramp in the Eastern Cordillera Basin (Colombia): Evidence from sedimentary geochemical proxies and facies analysis

Huber A. Rivera [a,b,c,*], Jacobus P. Le Roux [b,c], L. Katherine Sánchez [d], Jorge E. Mariño-Martínez [a], Christian Salazar [e], J. Carolina Barragán [a]

[a] Escuela de Ingeniería Geológica, Facultad Seccional Sogamoso, Universidad Pedagógica y Tecnológica de Colombia, Colombia
[b] Departamento de Geología, Facultad de Ciencias Físicas y Matemáticas, Universidad de Chile, Plaza Ercilla 803, Santiago, Chile
[c] Andean Geothermal Center of Excellence, Plaza Ercilla 803, Santiago, Chile
[d] Departmento de Ingeniería de Minas, Facultad de Ciencias Físicas y Matemáticas, Universidad de Chile, Tupper 2069, Santiago, Chile
[e] Geología, Facultad de Ingeniería, Universidad del Desarrollo, Santiago, Chile

ARTICLE INFO

Article history:
Received 11 March 2018
Received in revised form 2 May 2018
Accepted 3 May 2018
Available online 9 May 2018

Editor: Dr. B. Jones

Keywords:
Siliciclastic carbonate ramp
Tempestites
Redox-sensitive elements
Palaeoproductivity
Black shales

ABSTRACT

The Cretaceous black shales of Colombia are among the most important successions in the north of South America and have attracted the attention of many geoscientists and exploration companies over the last few decades, because of their high hydrocarbon potential and the presence of emerald deposits. However, many uncertainties still remain with regard to their tectonic setting, sequence stratigraphy, depositional environments, palaeoxygenation conditions, and organic matter preservation. In order to develop a more integrated picture of these different processes and conditions, we conducted a detailed sedimentological, inorganic geochemical (U, V, Ni, Zn, Mn, Fe, Ti, Mo, Cu, Cr, Cd, Ba) and sequence stratigraphic analysis of the Cretaceous black shales in the Magdalena-Tablazo Sub-Basin (Eastern Cordillera Basin) of Colombia. Eleven lithofacies and five lithofacies associations of a storm-dominated, siliciclastic-carbonate ramp were identified, which range from basin to shallow inner ramp environments. These facies were grouped into six third-order stratigraphic sequences showing high-order cycles of marine transgression with constrained regressive pulses during the late Valanginian to early Coniacian. The black shales succession represents deposition under anoxic bottom water with some intervals representing dysoxic-suboxic conditions. The evolution of the sedimentary environments and their palaeoxygenation history reflect tectonic and eustatic sea-level controls that 1) produced a variable orientation and position of the coastline throughout the Cretaceous; 2) conditioned the low-gradient ramp geometry (<0.3°) and 3) modified the oxygenation conditions in the Magdalena-Tablazo Sub-Basin. An improved understanding of the sedimentary setting during deposition of the Cretaceous black shales in the Magdalena-Tablazo Sub-Basin assists in highlighting the interplay between the mechanism of sedimentation and continuum anoxic conditions prevailing in a basin, as well the important role of nutrient input from continental runoff as a trigger of high productivity and extended anoxia conditions.

1. Introduction

The Cretaceous is recognized as a period of important plate-tectonics, long-term sea-level rise, and environmental, climate (greenhouse conditions) and biodiversity changes, among others. One of the most prominent of these patterns in the stratigraphic record is an interoceanic-interbasinal (rather than global) deposition of organic carbon-rich facies commonly associated with Oceanic Anoxic Events (OAE's) (Jenkyns, 2010; Trabucho-Alexandre et al., 2010). Although the fine-grained nature of the organic carbon-rich strata have hindered their study in terms of sedimentology, sequence stratigraphy, non-conventional hydrocarbons reservoir characterization and stratigraphic correlation tasks, they have attracted the attention of geologist as they host significant mineral and hydrocarbon resources and also provide invaluable information on the palaeoenvironmental conditions, including oxygenation-redox conditions, palaeoproductivity and organic matter enrichment.

* Corresponding author at: Departamento de Geología, Facultad de Ciencias Físicas y Matemáticas, Universidad de Chile, Plaza Ercilla 803, Santiago, Chile
E-mail address: huber.rivera@ug.uchile.cl. (H.A. Rivera).

https://doi.org/10.1016/j.sedgeo.2018.05.003
0037-0738/

In northern South America, the widespread occurrence of Cretaceous black shales and bituminous limestone deposits that contain proxy evidence for seafloor anoxia, including a lack of benthic organisms, an absence of bioturbation and enrichment in certain redox-sensitive trace elements, have been well documented. These black shale strata of the Eastern Cordillera Basin of Colombia offer an opportunity to study the palaeoenvironmental conditions of this organic-rich interval and to assess their variability of depositional systems and related palaeoredox behaviour through time during a long-term subsidence and transgressive interval (Fabre, 1983a, 1983b; Villamil, 1993).

In this study, we focus on the Cretaceous black shale and pelagic limestone/marlstone organic carbon-rich succession of the Eastern Cordillera Basin of Colombia, particularly in the Magdalena-Tablazo Sub-Basin, where the uppermost Rosablanca, Paja, Simití, Simijaca, La Frontera, and lower Conejo Formations, encompass a time interval ranging from latest Valanginian to early Coniacian (Fig. 1). We present sedimentological and high-resolution inorganic geochemical data as proxies for reaching three primary goals. First, on a regional scale, to provide a lithostratigraphic, sedimentological and inorganic geochemistry synthesis of the late Valanginian - early Coniacian black marine shale interval of the Eastern Cordillera Basin of Colombia and contribute to a better understanding of facies changes of this succession that has been hitherto studied mainly from a biostratigraphic point of view (e.g., Etayo, 1968; Etayo et al., 1976; Villamil and Arango, 1998; Patarroyo, 2009). On a wider scale, the second goal is to integrate sedimentological and sequence stratigraphic analyses to enhance our understanding of fine-grained sedimentary systems and also to interpret the palaeoenvironment, while unraveling the controlling processes responsible for this thick organic-rich black shale interval. The third goal is to ascertain whether sluggish ocean circulation, primary palaeoproductivity or a combination of both factors formed the primary control on the preservation of the organic matter, which will help to interpret the palaeo-oxygenation conditions at the site of deposition.

2. Geological setting

The Eastern Cordillera Basin is a fold-belt thrust eastward onto the edge of the Eastern Llanos Basin and westward onto the edge of the Middle Magdalena Basin (Fabre, 1983a). During the Mesozoic, the Eastern Cordillera Basin was an extensional basin (Sarmiento-Rojas et al., 2006) linked to the separation between North and South America and the formation of the proto-Caribbean (Cooper et al., 1995), as well as to back-arc extension east of the Central Cordillera. The latter was generated by subduction of the Farallon Plate beneath South America (Taboada et al., 2000). According to Fabre and Delaloye (1983), extensional and continental rifting in the Eastern Cordillera Basin, related to thinning of the crust during the Early Cretaceous, could have been active already in the Triassic-Jurassic, during which volcanic facies were deposited in these extensional basins. The detailed Cretaceous plate tectonic setting is still unresolved, however, with some authors favouring back-arc extension, others a passive margin, and still others intracontinental rifting related to the opening of the proto-Caribbean (see Sarmiento-Rojas et al., 2006 for further details). Nevertheless, for the latest Cretaceous (post-Santonian), all authors agree that a convergent margin existed west of Colombia (Sarmiento-Rojas et al., 2006) and that this extensional basin was inverted, deformed and uplifted during the Neogene.

<table>
<tr><th>Epoch</th><th>Age</th><th>MMB nomenclature</th><th>This study</th><th colspan="2">Villa de Leyva area nomenclature</th></tr>
<tr><td rowspan="6">Upper Cretaceous</td><td>Coniacian</td><td>Umir</td><td>Guadalupe Gr.</td><td colspan="2">Plaeners</td></tr>
<tr><td rowspan="3">Turonian</td><td rowspan="4">La Luna</td><td>Conejo</td><td colspan="2">Conejo-(Cucaita Member)</td></tr>
<tr><td>La Frontera</td><td rowspan="2">San Rafael</td><td>B</td></tr>
<tr><td>Simijaca</td><td>A</td></tr>
<tr><td>Cenomanian</td><td>Arenisca de Chiquinquirá</td><td colspan="2">Churuvita</td></tr>
<tr><td rowspan="8">Lower Cretaceous</td><td rowspan="2">Albian</td><td>Simití</td><td>Simití</td><td colspan="2">San Gil Superior</td></tr>
<tr><td>Tablazo</td><td>Tablazo</td><td colspan="2">San Gil Inferior</td></tr>
<tr><td>Aptian</td><td rowspan="3">Paja</td><td rowspan="3">Paja</td><td colspan="2" rowspan="2">Paja</td></tr>
<tr><td>Barremian</td></tr>
<tr><td>Hauterivian</td><td colspan="2">Ritoque</td></tr>
<tr><td>Valanginian</td><td>Ritoque</td><td rowspan="3">Rosablanca</td><td colspan="2">Rosablanca</td></tr>
<tr><td rowspan="2">Berriasian</td><td rowspan="2">Rosablanca</td><td colspan="2">Arcabuco</td></tr>
<tr><td colspan="2"></td></tr>
</table>

Fig. 1. Cretaceous sedimentary succession with ages showing correlation of nomenclature of formations used within adjacent basins and areas.

The Magdalena-Tablazo Sub-Basin formed as an NNE-SSW-trending hemi-graben, separated from the Cocuy Sub-Basin by the Santander-Floresta Paleomassif (Fig. 2) (Fabre, 1983b; Cooper et al., 1995; Sarmiento-Rojas et al., 2006). Its origin probably dates back to the Late Jurassic as a product of crustal thinning (Fabre, 1983a, 1983b). Sedimentation started with marine flooding from south to north, and palaeontological evidence of a Berriasian–Valanginian age proposed by McLaughlin (1972) for some evaporite occurrences strengthens the idea of an arid palaeoenvironment preceding the transgression (Bürgl, 1967). Both sub-basins linked up to form a single, wide basin during the Hauterivian due to flooding of the Santander-Floresta Palaeomassif (Fabre, 1983b). However, this intrabasinal high constituted a significant barrier controlling sedimentation until the Aptian (Sarmiento-Rojas et al., 2006). The deposition of shelf carbonates was dominant during the Valanginian - Hauterivian, forming the Rosablanca Formation (Cardozo and Ramírez, 1985). This was succeeded by the black shales of the Paja Formation during the Hauterivian - Barremian (Etayo et al., 1976), indicating a stagnated, shallow-marine environment. However, during the late Aptian, the Paja Formation developed deeper facies in response to a relative tectono-eustatic rise in sea-level (Forero and Sarmiento, 1985). Thus, the cycle corresponds to typical *syn*-rift sedimentation.

The post-rift deposition is characterized by an initial relative sea-level fall followed by transgression (Villamil, 1993), causing a transition from near-shore facies of the Tablazo Formation (Fig. 1) to outer shelf facies of the Simití Formation. Subsequently, during the earliest Cenomanian, a forced regression is interpreted by Villamil (1998) at the base of the Churuvita Formation near the Villa de Leyva area (see Fig. 2), which is time-equivalent to the shallow-water sandstone of the Areniscas de Chiquinquirá Formation (Fig. 1). The latter is corroborated by observations of Guerrero (2002) and Terraza (2012), who placed a sequence boundary related to a relatively fast sea-level fall at the base of Cenomanian strata in the upper Une allomember and segment C of the Areniscas de Chiquinquirá Formation, respectively. Around the late Cenomanian - Turonian boundary, the entire Eastern Cordillera Basin registered a maximum flooding surface, indicated by a slight deepening of the basin and a marked decrease in the supply of coarser continental clastics (Sarmiento-Rojas et al., 2006), which allowed the deposition of dark muds of the Simijaca and La Frontera Formations. This was followed by gradual progradation and shallowing during the deposition of the uppermost part of the Conejo Formation, related to a normal regression linked to a sea-level high stand.

Regarding the stratigraphic nomenclature, the Simití Formation described here corresponds to the San Gil Superior Formation (sensu Etayo, 1968), whereas the Simijaca and La Frontera Formations correspond to Segments A and B of the San Rafael Formation (sensu Etayo, 1968), respectively. The correlation and chronostratigraphy of the studied Cretaceous succession are indicated in Fig. 1, whereas Figs. 3 and 4 show the stratigraphic columns of the complete succession measured in this study.

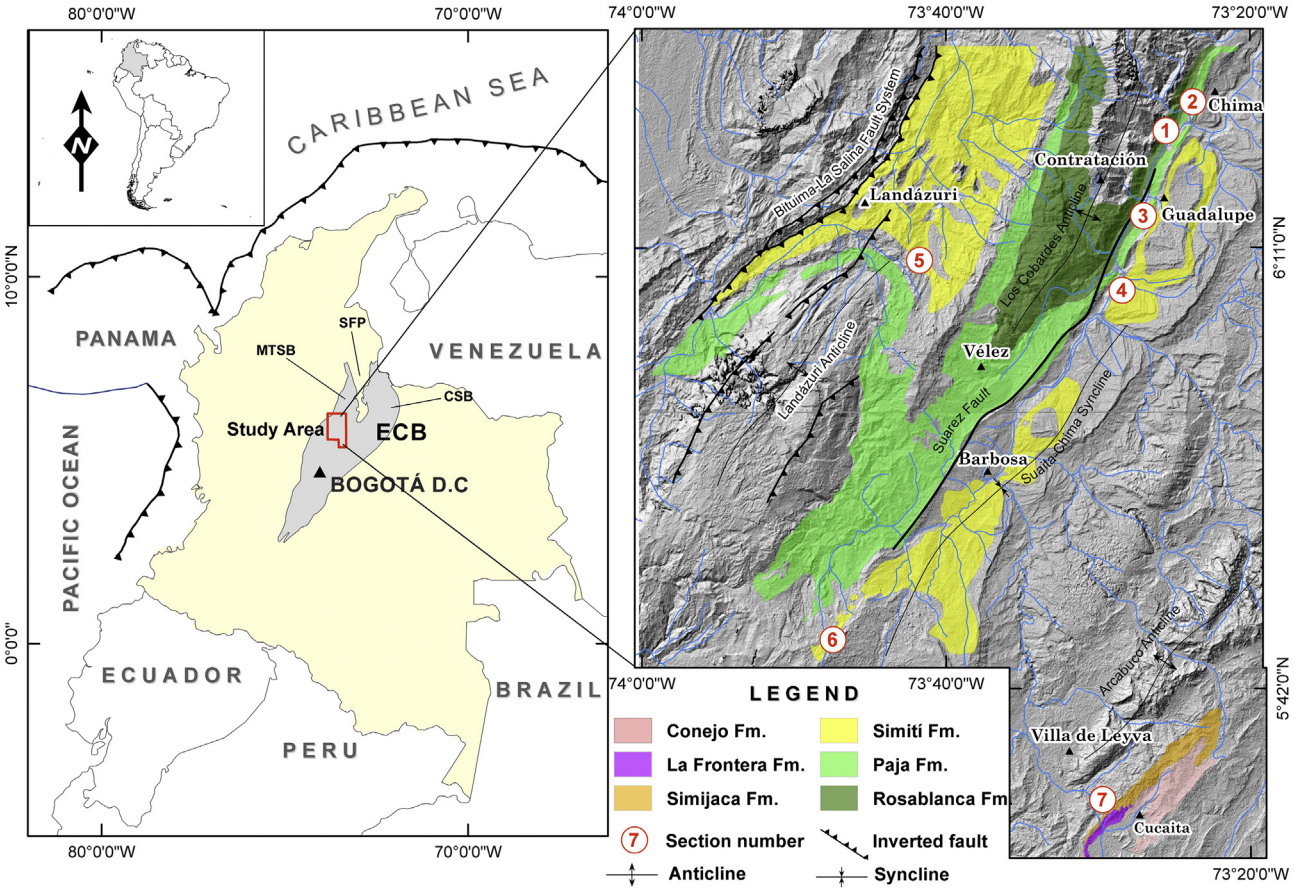

Fig. 2. Simplified geological map of the Eastern Cordillera Basin (ECB), showing the location of the study area and measured stratigraphic sections mentioned in the text. Note how the Santander-Floresta Palaeomassif (SFP) separates the Magdalena-Tablazo Sub-Basin (MTSB) from the Cocuy Sub-Basin (CSB).

3. Sampling and methods

3.1. Lithostratigraphy, sedimentology and sequence stratigraphy

A total of seven stratigraphic sections (Table 1; Fig. 2) were measured in the Magdalena-Tablazo Sub-Basin at a scale of 1:200, using a Jacob staff and measuring tape, totaling ~1 km in thickness. The description of lithofacies is based on a careful examination of outcrops on a cm/dm scale, defining facies according to their bed geometry, contacts, lithology, sedimentary structures, textures, fossils (including some taphonomic aspects), and trace fossils. Carbonate facies were defined according to Dunham (1962) and siliciclastic facies according to their physical and biological attributes.

Sequence stratigraphic units and systems tracts were defined from flooding or transgressive surfaces (TS), subaerial unconformities or sequence boundaries (SB) and maximum flooding surfaces (MFS). As the sequence stratigraphic framework presented in this study is entirely based on outcrop data, where the geometry of stratigraphic sequences cannot be identified with certainty due to the absence of regional correlation plots, some sequence stratigraphic surfaces may have been missed. Moreover, in deeper water, the MFS is in most cases ambiguously identified. Despite these limitations, we have defined stratigraphic sequences characterized by the development of two or three systems tracts in the sense of Catuneanu et al. (2011): a lower transgressive tract (TST), and an upper, shallower, highstand systems tract (HST), in deeper water settings. In shallower parts of the sedimentary system, it is also possible to define a third, lowstand systems tract (LST) where a basal subaerial unconformity can usually be recognized. The LST includes deposits accumulated during normal regressions and is bounded by a basal subaerial unconformity (SB) and a flooding or transgressive surface (TS) at the top. The transgressive systems tract begins with a TS characterized by transgressive shell lag or a condensed shell bed, that resulted from low net deposition due to sediment bypass, typically accompanied by a deepening-upward trend of facies (Zecchin and Catuneanu, 2013, 2017). Where subaerial unconformities are not present (particularly in deeper water settings), the TS is used as a sequence boundary. The HST is accompanied by a shallowing-upward trend of facies and is separated from the underlying TST by the maximum flooding surface (MFS), that is characterized by the development of nodular horizons (incipient hardground), a high concentration of pyrite and organic matter, phosphate layers and sometimes intense bioturbation.

3.2. X-ray fluorescence (XRF) and trace element ratios

In order to define changes of the water-mass palaeoxygenation conditions during sedimentation, ca. 2000 measures of major element oxides and trace element concentrations were determined by X-ray fluorescence, using a handheld Thermo Scientific Niton XL3t analyzer equipped with a silicon drift detector and calibrated on pressed powder pellets with the use of a He purge system. The sampling was at intervals of 50 cm for each of the seven stratigraphic columns (Table 1; Figs. 3 and 4) and all the analyses were performed on fresh and washed surfaces to avoid surficial contamination and to obtain precision errors in the order of 3–5%. Counting times were 30 s on the low, main and high energy filters (for analyzing minor and trace elements in ppm), and 90 s on the light filter setting (for analyzing major elements in wt%) for a total of 180 s. Additionally, 2–3 system checks were carried out daily.

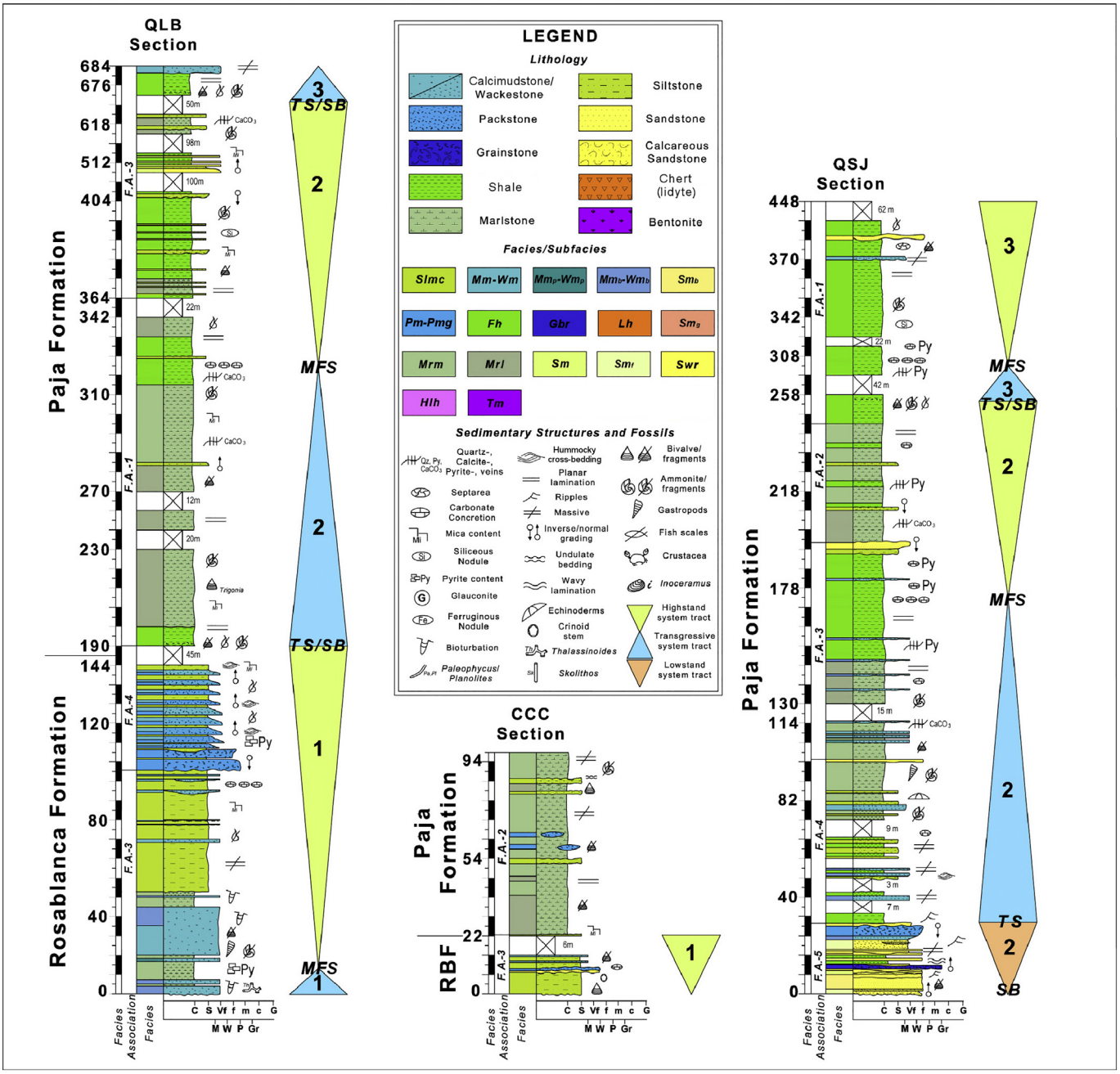

Fig. 3. Stratigraphic profiles of the Rosablanca and Paja Formations, illustrating facies, facies associations and interpreted sequence stratigraphic framework. RBF = Rosablanca Formation. For location, see Fig. 2.

In this paper we follow the redox classification scheme proposed by Tyson and Pearson (1991): oxic, dysoxic, suboxic, anoxic, and euxinic conditions. Rivera et al. (2016), by means of a cross-plot of redox-sensitive trace elements versus titanium, which is indicative of detrital origin and usually immobile during diagenesis, determined that in most cases only Ni, V, and U are reliable indicators of redox conditions for the Magdalena-Tablazo Sub-Basin, whereas Cr, Co are controlled by the detrital input. In this study, we used V/Cr and V/(V + Ni) ratios to evaluate palaeoredox conditions, and the (Fe + Mn)/Ti ratio as an indicator to evaluate the hydrothermal influence on sedimentation, which might have provided a significant amount of redox-sensitive elements to the system. The V/Cr, V/(V + Ni) and (Fe + Mn)/Ti ratios are based on Jones and Manning (1994), Hatch and Leventhal (1992) and He et al. (2016), respectively. V/Cr ratios of <2 indicate oxic conditions, 2–4.25 dysoxic conditions, and >4.25 suboxic to anoxic conditions; V/(V + Ni) ratios >0.84 indicate euxinic conditions, 0.54–0.82 anoxic and 0.46–0.60 dysoxic conditions; (Fe + Mn)/Ti values >15 typically indicate a hydrothermal influence, while lower values suggest that the influx of terrigenous material was more representative than that of hydrothermal sources.

In order to determine the origin of organic matter based on trace elements, we applied the V/Ni ratio proposed by Galarraga et al. (2008) to characterize both the palaeoenvironmental conditions of the source rocks and the origin of precursor organic matter. A V/Ni ratio higher than 3 reflects anoxic conditions during deposition of organic matter with a marine origin, values ranging from 1.9 to 3 indicate deposition under dysoxic-oxic conditions with organic matter of a mixed terrestrial and predominantly marine origin, and values lower than 1.9 show a terrestrial origin of organic matter under prevailing oxic conditions during deposition.

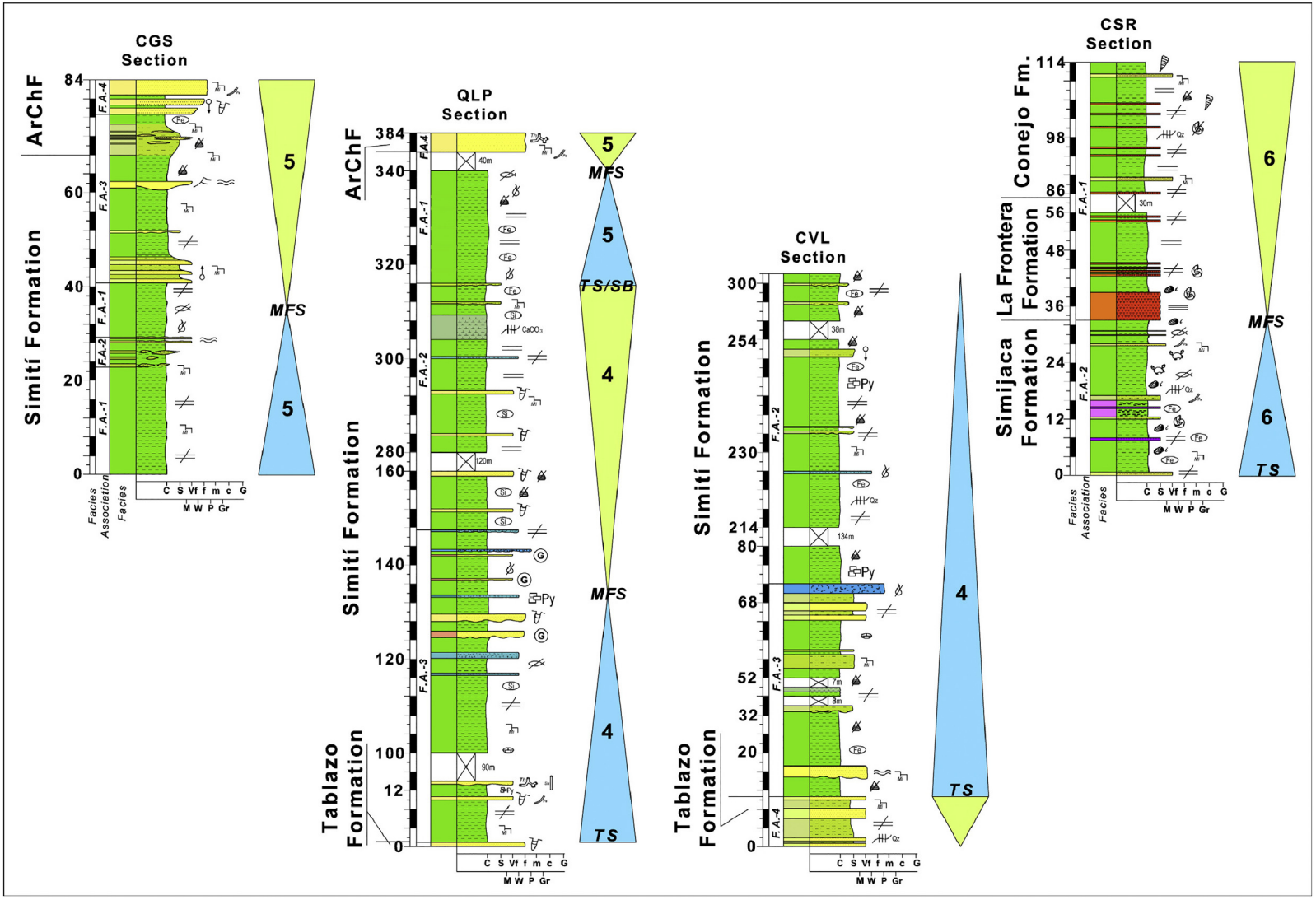

Fig. 4. Stratigraphic profiles of the Simití, Simijaca, La Frontera and Conejo Formations, illustrating facies, facies associations and interpreted sequence stratigraphic framework (For location, see Fig. 1). ArChF = Areniscas de Chiquinquirá Formation. Legend as indicated in Fig. 3.

Table 1
List of originally measured sections and present designation numbered from 1 to 7. The three sets of letters indicate the abbreviation of each section.

Section number	Name	Abbreviation
1	Carretera Chima - Contratación	CCC
2	Quebrada San José	QSJ
3	Quebrada La Bosqueña	QLB
4	Quebrada La Pava	QLP
5	Carretera Vélez - Landázuri	CVL
6	Carretera Garavito - Sabaneta	CGS
7	Chircal San Rafael	CSR

4. Results and discussion

4.1. Facies analysis and palaeoenvironmental interpretation

Carbonate, siliciclastic and mixed rocks were recognized in the measured sections and correspond to eleven different facies (Table 2). The latter have been grouped together into recurring, genetically related facies, which are described below.

4.1.1. Facies association 1: Basin

This facies association is dominated by low energy-facies, including black, well-laminated bituminous shale (Fh) (Fig. 5a), locally intercalated with elongated, ferruginous nodules (Fig. 8c) and fibrous calcite (shale beef structures) with bituminous inclusions (Fig. 8a). This facies normally occurs in tabular units ranging between 1 and >12 m thick, which show sharp, planar contacts. There are also gray to black, massive to laminated marlstone (Mrm, Mrl), with tabular geometry and thicknesses from centimeters to tens of meters, showing sharp basal and upper contacts. The thicker units grade internally from black, laminated shale (Fh) to massive, bituminous marlstone (Mrm) and some diagenetic nodules and concretions (Fig. 8b) are present. Interbedded organic matter-rich, thin siltstones (Slmc) or sandstones with wavy lamination and ripple marks (Swr) and massive calcimudstone to massive, pyrite-rich calcimudstones (Mm, Mm_p) also occur sporadically. Tabular, laterally continuous, well-stratified laminated chert facies (Lh) is very common in the La Frontera and lower Conejo Formations, characterized by internal, fine laminae (1–3 mm), in which silicified, finely-laminated shales (Fh) and siltstones (Slmc) alternate. Where siltstones dominate, wispy laminated sandstone can also be present (Fig. 5g), in which case the contacts are slightly erosional. Double-mud layers are also common, consisting of two mud drapes (Fig. 5f) with a sandy or silty bed in-between. The fossil content in the overall facies association is generally scarce, although some horizons rich in bivalves and ammonites are present. Among the most common genera of ammonites are moderate to well-preserved *Hoplitoides* sp. (Fig. 6d) and *Parahoplites?* sp. (Fig. 6b). There are also gastropods, echinoderms up to 8 cm in diameter, fish scales, and rare, well-preserved examples of *Trigonia* (*Quadratotrigonia*) *hondaana* Lea (Darío Lazo, pers. com., 2016; Fig. 6c). Bioturbation is very scarce to absent. This facies association is dominant in the Paja, Simití, La Frontera and Conejo Formations.

The lamination displayed by this fine-grained facies (Fh, Mrl) (Fig. 5a), indicates deposition from suspension in stratified water, whereas the black color, high organic content, and abundance of pyrite imply reducing conditions in a very low-energy environment below the storm wave base (Spalletti et al., 2000, 2001; Kietzmann et al., 2008, 2014, 2016). On the other hand, facies Mrl, Mrm indicate enhanced carbonate production and a low clastic input (Spalletti et al., 2001; Kietzmann et al., 2008). The elongated ferruginous nodules (Fig. 8c) are probably related to early diagenetic processes in which rapid sulfate reduction occurred in the presence of high concentrations of active iron in a poorly-oxygenated environment. These oxygen-depleted conditions also prevented the proliferation of benthic organisms that would have destroyed the primary structures. On the other hand, the shale beef structures (Fig. 8a) are related to overpressure during the migration of hydrocarbons that together with watery fluids, dissolve, transport and precipitate calcite to generate these structures at great depths (Rodrigues et al., 2009; Cobbold et al., 2013).

Laminated chert (Lh) suggests a tranquil environment with deposition mainly from suspension. However, the slightly erosional contacts between siltstone-sandstone laminae (Fig. 5g) also indicate low-intensity currents, and where intercalated with black, laminated bituminous shale (Fh). This facies is interpreted as silty contourites sensu Rebesco et al. (2014) that were reworked from distal turbidites or tempestites. The formation of contourites is related to the constant displacement of water masses along the ocean floor, probably via barotropical or baroclinical currents (Shanmugam, 2013) and according to Villamil (1996) upwelling currents were very common together with Ekman forces during much of the Cretaceous in the Eastern Cordillera Basin. The possibility that upwelling currents could have interacted with density flows triggered by storms is not ruled out, which fits in very well with the sedimentological model.

Diagenetic nodules and concretions represent "incipient hardground" (Christ et al., 2015), widely associated with very low sedimentation rates or interruptions in sedimentation for a variable length of time. Their occurrence as laterally continuous cemented bodies or hardground intervals (Fig. 8b) is commonly associated with major marine flooding surfaces (or maximum flooding surfaces) (Aurell, 1991; Taylor et al., 2000; Ketzer et al., 2003; Taylor and Machent, 2010).

The siltstone beds (Slmc) or sandstones with wavy lamination and ripple marks (Swr), also rich in organic matter and without signs of bioturbation, represent episodic events forming distal tempestites (Fig. 9b) at times when siliciclastic sedimentation was favoured (Kietzmann et al., 2008).

Facies association 1 (indicated by 1, in Fig. 10) reflects a low energy environment dominated by slow suspension deposition of terrigenous particles and plankton in the stratified water, rarely interrupted by distal density flows triggered by storms.

4.1.2. Facies association 2: distal outer ramp to basin

The dominance of low-energy facies of this association is similar to those of facies association 1, including thick, massive to laminated marlstone (Mrm, Mrl) showing tabular geometry and slightly erosional bases in cases where this facies is associated with massive sandstones (Sm), thick, black, laminated bituminous shale (Fh) (Fig. 5a) with fissile weathering, sub-tabular geometry and sharp to undulate contacts. These are frequently intercalated with lenses of bivalve and small ammonite fragments, and thin, laterally continuous beds with abundant gastropods, brachiopods, and disarticulated bivalves. There are also massive to vaguely laminated, tabular to lenticular siltstones (Slmc), sometimes with undulate upper contacts, massive calcimudstone-wackestone (Mm-Wm) and massive, pyrite-rich calcimudstone-wackestone (Mm_p-Wm_p) the latter showing, disoriented fossil fragments. More rarely beds of massive to bioturbated sandstone (Sm, Sm_b), massive, altered bentonites (Tm), and shale with isolated sandstone ripple marks (Hlh) (Fig. 5e) may be present. The pyrite content is dispersed throughout this facies association and the faunal diversity is low, with autochthonous bivalves and ammonites adapted to poorly oxygenated environments and preserved as internal molds and impressions. Some well-preserved examples of the crustacean *Cenomanocarcinus vanstraeleni* (Fig. 6a) can be found, together with *Inoceramus* sp., *Mytiloides labiatus* (Fig. 6g) and *Hoplitoides* sp. (Fig. 6d). The ichnofossil diversity is also restricted, but *Thalassinoides* isp. (Fig. 7a, b), *Taenidium* isp. (Fig. 7e) and *Planolites* isp. can be recognized. Rarely, 15–30 cm thick siltstone/sandstone beds are interconnected with each other by a clastic injectite network, which occurs oblique or orthogonal to the stratification (Fig. 9d). This facies association is dominant in the Paja, Simití and Simijaca Formations.

The main depositional process for this facies association was suspension accretion of calcareous and siliciclastic muds below the storm wave base in a low-energy environment (indicated by 2, in Fig. 10). The more

Table 2
Facies descriptions with summarized sedimentological features and sedimentary interpretation of the mixed siliciclastic-carbonate homoclinal ramp of the Magdalena-Tablazo Sub-Basin. Italic letters indicate sub-facies.

Code	Fossils and taphonomy	Sedimentary structures–bioturbation–composition	Geometry–contacts–color–thickness	Interpretation of sedimentary processes
Fh	Scarce fossils, some horizons rich in bivalve imprints, rarer gastropods and echinoderms molds. *Inoceramus* sp., *Mytiloides labiatus*, *Hoplitoides* sp., *Cenomanocarcinus vanstraeleni*	Finely laminated to fissile–low to null bioturbation–siliceous and bituminous; cross-cutting pyrite-filled veins	Tabular–sharp to rarely undulate (wavy) contacts–black to medium gray–50 cm up to 12 m	Deposition by suspension and vertical settling in very low to moderated energy and poorly-oxygenated environments below of storm-wave base level. Related to distal diluted gravitational flows, induced by storm waves; fossil-rich horizon is interpreted as a condensed section
Slmc	Bivalves (Family Lucinidae) of mm-scale, well-preserved and generally articulated, while larger ones (<5 cm), show some signs of abrasion	Massive to poorly laminated; HCS–low bioturbation: *Palaeophycus* isp.–Calcareous and siliceous	Tabular to lenticular–sharp to erosive contacts–light gray–up to 20 m	Sedimentation by fast vertical settling in low to moderated energy environments with low oxygen levels; distal turbidites related to storms episodes; small channels that usually cross sea floor related to storm surge
Lh	Scarce foraminifers and gastropods, occasional well-preserved *Hoplitoides* sp.	finely laminated, wispy lamination and double mud layers–null–Siliceous (lydite)	Tabular–sharp contacts–beige to reddish-beige–l 15 to 50 cm, 6 m	Sedimentation by suspension in low flow regimes with low current intensity; tractive processes, alternating low and moderate current intensity on the sea floor in poorly oxygen conditions
Hlh	Absent	Heterolithic lenticular–null bioturbation–siliceous, bituminous	Lenticular–sharp contacts–dark gray to black–up to 1.5 m	Sudden shift between stationary water conditions and turbulent regimes, where sediment starvation exists. Related to whether waning stages of hyperpycnal or to tidal bottom currents
Sm Sm_f-Sm_b Sm_g	Millimetric, highly fragmented bivalves, and gastropods. Centrimetric ammonites forming shell lag deposits on erosional contacts, arranged in decreasing-upwards size	Massive, normal and inverse grading–mottled, *Skolithos* isp., *Planolites* isp., *Taenidium* isp. *Thalassinoides* isp.–Siliceous, calcareous locally, and glauconitic	Sub-tabular and amalgamated to lenticular–erosive base, sharp upper contacts–grayish to pale yellow–10 cm up to 1 m	Rapid accumulation of sand from sediment gravity flows in offshore areas triggered by storms; deposition under conditions of rapid flows carpet shear (fraction- carpet); fast accumulation of sand and shells in channels by high-energy events related to storms
Swr	Sparse fossil. Some fragmented bivalves	Current ripples, wavy lamination–low bioturbation–Siliceous and mica-rich	Tabular, channel form–sharp base to slightly erosional, wavy upper contact–light to dark gray–50 cm up to 2 m	Intense oscillatory flows with reduced unidirectional component or combined flows; alternating traction currents in lower flow regime with vertical accretion processes during sedimentation of distal turbidites or tempestites
Mrm *Mrl*	Rarely, lenses-filled of mm-scale bivalves and echinoderms. A well-preserved *Trigonia* (*Quadratotrigonia*) *hondaana* Lea. Thin, laterally continuous beds with highly disarticulated and fragmented gastropods, brachiopods, and bivalves	Massive, incipient lamination (fissile)–low bioturbation–calcareous, mica-rich or pyrite-rich	Tabular–sharp contacts, rarely slightly erosive–black to light gray–30 cm up to >10 m	Sedimentation by suspension matching with periods of high carbonatic productivity in an anoxic-dysoxic, low energy environment; fossil-rich horizon is interpreted as diluted fluid gravity flows triggered by distant storms whereas small channels filled signal stronger storm currents closer to and perpendicular to the coastline
Mm-Wm Mm_p-Wm_p Mm_b-Wm_b	Bivalves, *Lissonia* sp., *Nicklesia* sp., unidentified fossils fragments in a random way and occasionally parallel to bedding	Massive; HCS–mottled, *Thalassinoides* isp.–calcareous	Tabular, lenticular–sharp contacts, erosive bases–grayish–50 cm up to 15 m	Deposition from fast suspension fall out of large amounts of carbonated mud, probably re-suspended by storms under energy to calm water conditions
Pm *Pmg*	Bivalves with thin shells are generally articulated and moderately fragmented but disarticulated and more fragmented may also be present	Massive, normal and inverse grading–low bioturbation–calcareous	Tabular–sharp contacts to erosive bases–medium gray–20 cm to 2 m	High energy deposition generated under conditions of turbulent flows with a progressive decay of the flow regime; Related with bottom remobilization and reworking during storms
Gbr	Crinoids, bivalves, oysters and some ammonites, moderately fragmented and articulated, with a generally chaotic orientation but sometimes oblique or perpendicular to the bedding.	Massive, normal grading, ripples–poor to moderate bioturbation–calcareous	Sub-tabular–sharp and erosive contacts–grayish–2 m	Deposition of accretionary bioclastic shoals in a warm, well-oxygenated water with normal salinity above to the fair weather-wave base. Affected by conditions of turbulent flows related whether to storm or wave action
Tm	Absent	Massive–bioturbation absent–highly oxidized, siliceous	Tabular–sharp contacts pale yellow to whitish–25 to 50 cm	Very distal ash falls from eruptive plumes and/or distal, non-cohesive turbidity flows

frequent alternation with moderate-energy facies reflected by tabular to lenticular siltstones (Slmc) and massive calcimudstone-wackestone (Mm-Wm), suggests the action of tempestite flows in a distal outer ramp. On the other hand, sub-facies Mm_p-Wm_p could mark the transition from a loose, saturated to a more plastic substrate (Spalletti et al., 2001) under deficient oxygenation conditions, as indicated by the disseminated pyrite content and scarce bioturbation. However, the association of *Thalassinoides* isp., *Taenidium* isp., and *Planolites* isp. is indicative of the *Cruziana* ichnofacies (Pemberton and MacEachern, 1997; Buatois and Mángano, 2011) reflecting episodes of increased substrate oxygenation in an anoxic to suboxic open marine environment.

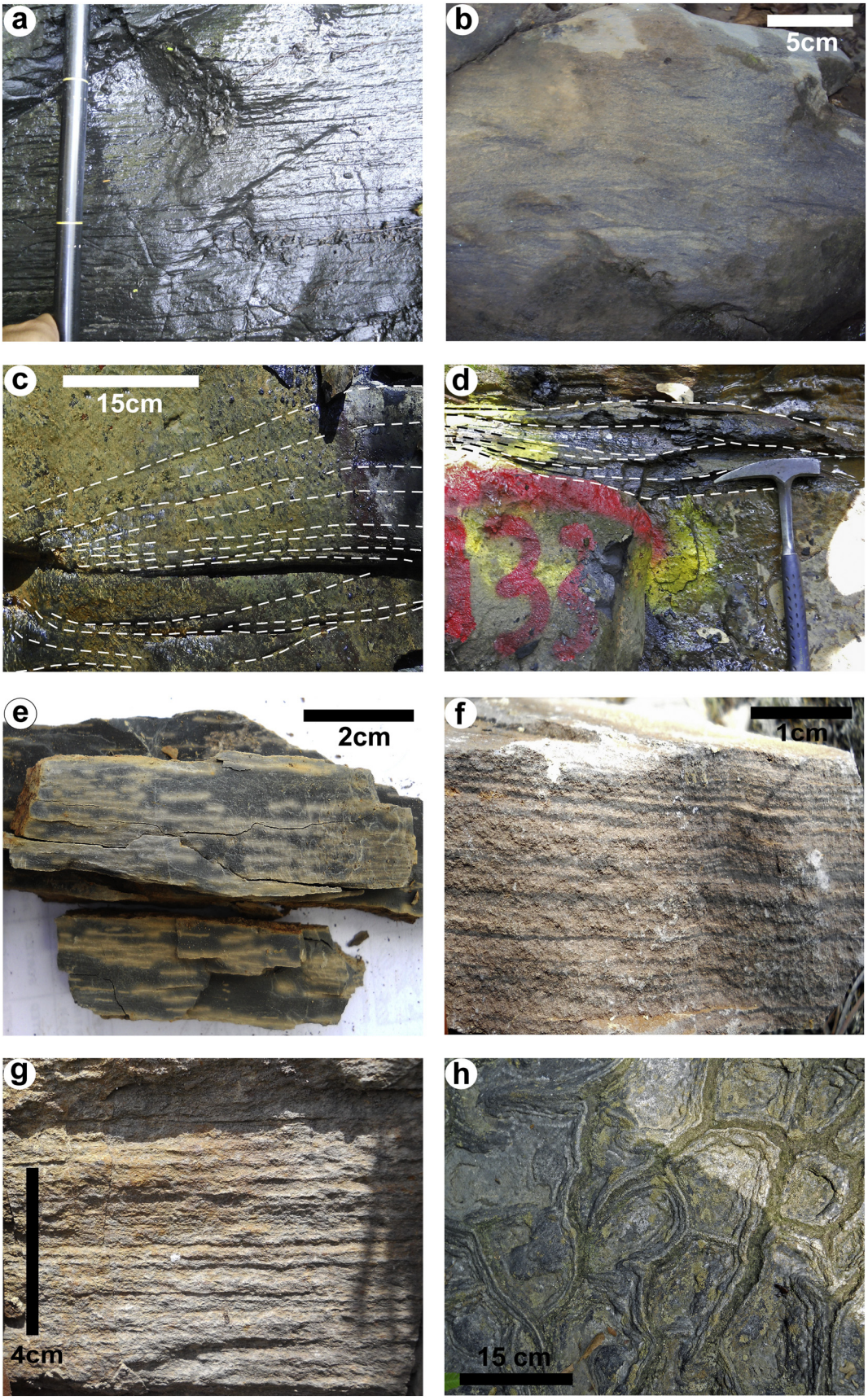

Fig. 5. (a) Black, bituminous shales with finely well-developed planar lamination (Facies Fh). Each mark in the Jacob staff is 10 cm long. (b) Unidirectional flow ripples on sandstone of the basal Paja Formation (QSJ section) (Facies Swr). (c) Remnants of Hummocky cross-stratification on bioturbated wackestone (Facies Wm_b). (d) Hummocky cross-stratification on bioturbated, siltstone (Facies Smlc). (e) Shale with isolated sandstone ripples (Facies Hlb). (f) Double mud layer in laminated chert (lydites) (Facies Lh). (g) Detail of wispy lamination in laminated chert facies (Lh). (h) Mud cracks developed in algal mats of the Tablazo Formation.

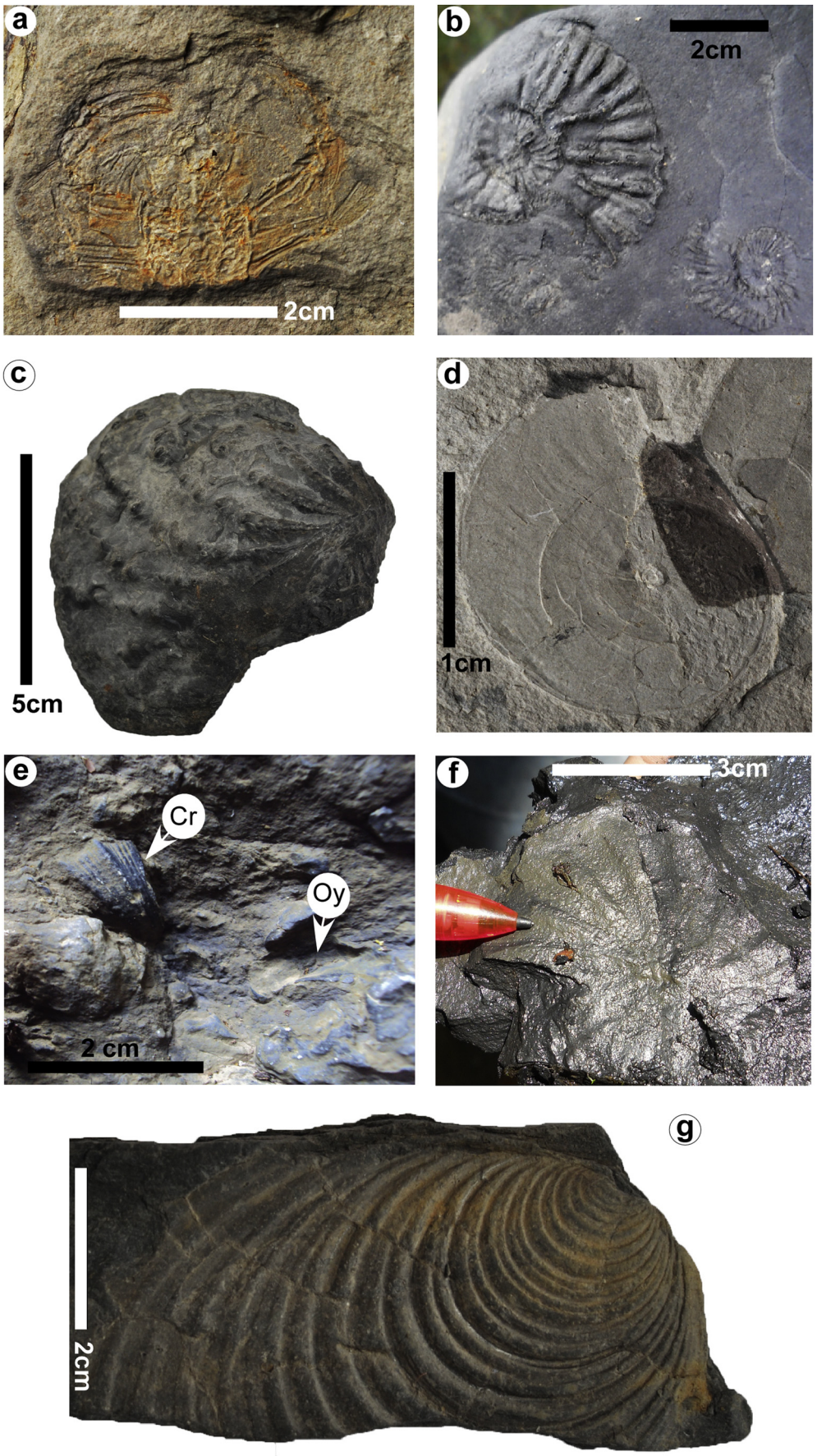

Fig. 6. Example of fossil assemblage of the studied succession. (a) *Cenomanocarcinus vanstraeleni*. (b) Molds of *Parahoplites?* sp. (c) Specimen of *Trigonia* (*Quadratotrigonia*) *hondaana* Lea. (d) *Hoplitoides* sp. (e) Crinoid stem (Cr) and oyster shell (Oy) on bioclastic grainstone facies (Gbc). (f) Echinoderm mold. (g) *Inoceramus* (*Mytiloides*) *labiatus*.

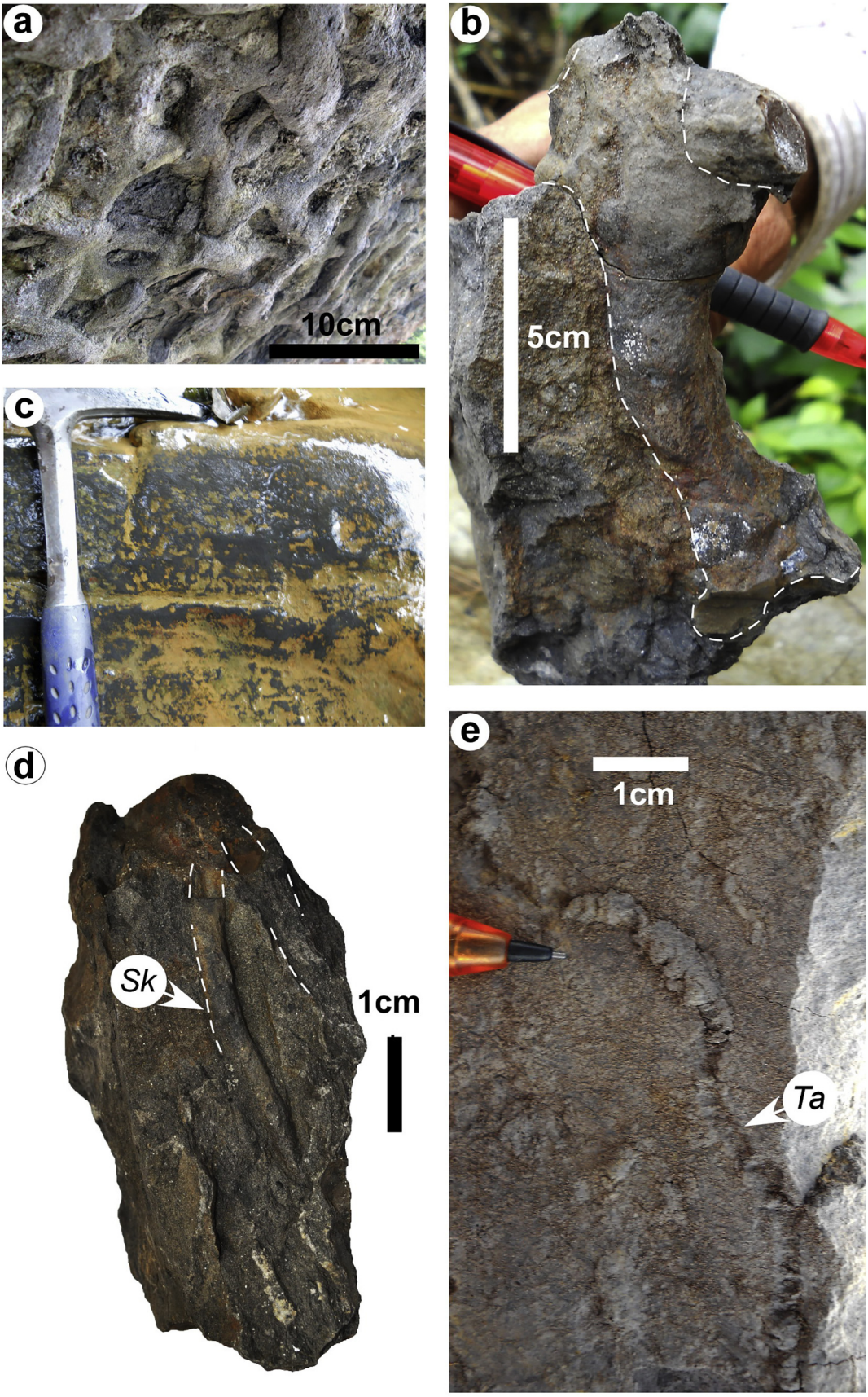

Fig. 7. Ichnofossil assemblage. (a) Bedding plane with abundant *Thalassinoides* isp. (b) A specimen of *Thalassinoides* isp. (c) Mottled structure of massive, calcimudstone-wackestone facies (Mm_b-Wm_b). (d) *Skolithos* isp. (e) *Taenidium* isp.

Massive, altered bentonites (Tm) can be interpreted as distal ash falls related to eruptive plumes. The shales with isolated sandstone ripple marks facies (Hlh) (Fig. 5e) can be interpreted as reflecting waning stages of hyperpycnal flows where large suspension loads reached distal parts of the ramp, or alternatively to deposition under oscillating flow probably induced by tidal bottom currents (Shanmugam, 2008 and references therein). However, due to the fact that both facies are strongly associated, they can be interpreted as distal, non-cohesive turbidity flows (Kietzmann et al., 2014). This could explain the episodes of better oxygenation. Other features such as injectite structures (Fig. 9d) observed in this facies association, suggest synsedimentary remobilization of silt/sand triggered by the rapid burial of isolated, porous sands within low permeability muds, or by the intrabasinal migration of hydrocarbons and/or groundwater.

4.1.3. Facies association 3: proximal outer ramp

The proximal outer ramp is dominated by siliciclastic and calcareous mud, represented by the black, bituminous, fissile-weathering shale (Fh), massive to laminated marlstone (Mrm-Mrl) facies. This facies also shows local shale beef structures (Fig. 8a), nodules and concretions (Fig. 8b) and calcareous, massive to laminated, occasionally clay-rich siltstones (Slmc) forming decimetric- to metric-scale (up to 20 m) tabular packages with sharp (sometimes slightly erosional) basal and upper contacts. These are intercalated with thin beds and lenses of calcimudstone-wackestone (Mm-Wm) with erosional bases that locally show a high percentage of pyrite (Mm_p-Wm_p), and occasional massive sandstone lenses (Sm). The main differences with respect to the distal outer ramp facies association are evidence for slightly better oxygenation, as well as abundant intercalations of siltstone (Slmc), massive to bioturbated calcimudstone-wackestone (Mm-Wm, Mm_b-Wm_b), massive, bioturbated and glauconitic sandstones (Sm, Sm_b, Sm_g), and sandstones with ripple and wavy lamination (Swr). Subordinate facies include thin beds of sandstone and siltstone with normal grading and massive bioclastic packstone (Pm), with rare normal gradation of the bioclasts. The latter consist of small echinoderms (Fig. 6f) and bivalves that are generally articulated or moderately fragmented, contrary to the larger bivalves that show signs of abrasion. Additional fauna include crinoids and ammonite fragments of *Nicklesia* sp. deposited parallel to the stratification. The sandstones are dominantly massive as a result of bioturbation (fodinichnia and domichnia) and recognizable trace fossils include the ichnogenera *Skolithos* isp. (Fig. 7d), *Planolites* isp., *Taenidium* isp. (Fig. 7e), and *Thalassinoides* isp. (Fig. 7a, b). Facies association 3 is dominant in the Paja and Simití Formations, and sub-dominant in the Rosablanca Formation.

This facies association (indicated by 3, in Fig. 10) reflects moderate to low energy conditions dominated by suspension accretion of plankton and allomicritic mud during periods of high productivity (Spalletti et al., 2001; Kietzmann et al., 2008). Siliciclastic muds (Slmc, Fh) indicate increased terrestrial input and the frequent intercalations with massive calcimudstone-wackestone (Mm-Wm) with erosional bases, massive sandstone lenses (Sm), and marlstone (Mrm-Mrl), suggest the transport of calcareous muds from shallow water. Sub-facies Mm_b-Wm_b, with its abundant bioturbation, signals a loose muddy substrate ideal for the colonization of benthic fauna under well oxygenated conditions (Spalletti et al., 2001). The trace fossils association is indicative of proximal *Cruziana* ichnofacies (Pemberton and MacEachern, 1997), which is characterized by the intense activity of detritivore organisms that lived in a well-oxygenated, tranquil environment where the benthic community developed under stable conditions. The massive packstone (Pm) beds, rarely showing a normal gradation of bioclasts (ranging from 0.25–0.5 mm in mean diameter), together with the fragmentation and disarticulation of bivalves, indicate turbulent (both oscillatory and unidirectional), waning flows probably associated with storms (Spalletti et al., 2000; Bádenas and Aurell, 2001; Kietzmann

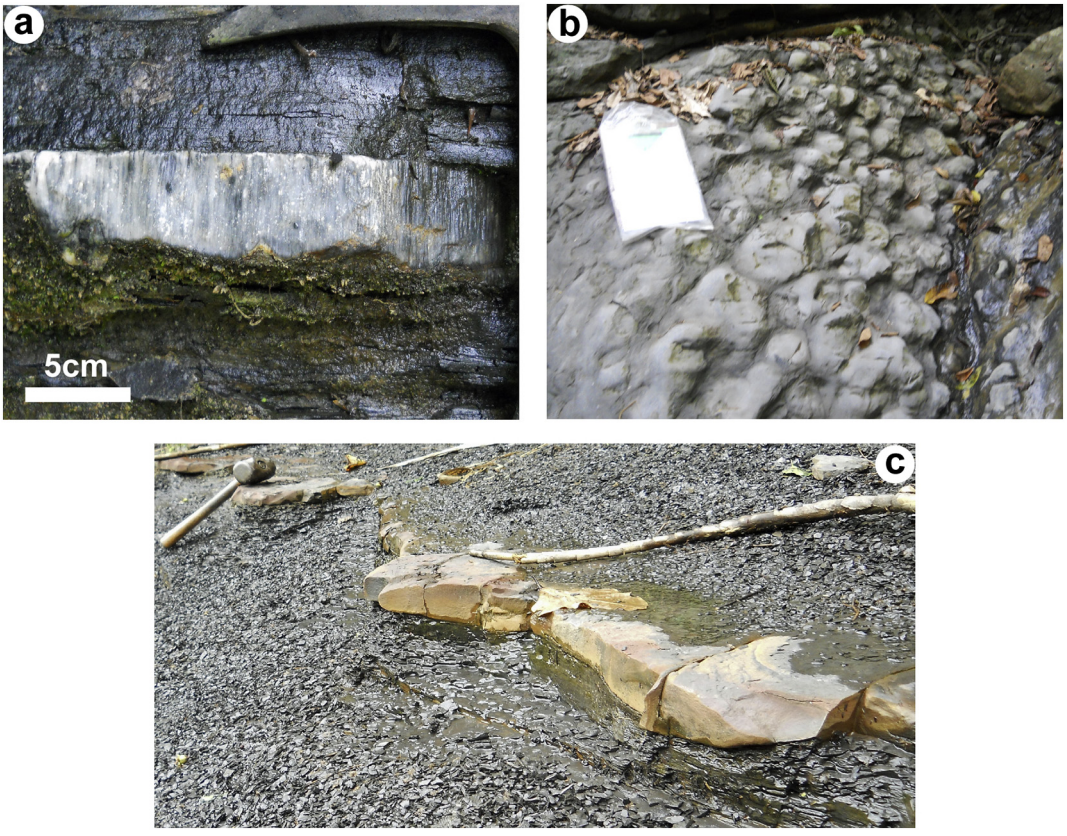

Fig. 8. (a) Bitumen inclusions in fibrous calcite (shale with beef structures). (b) Conspicuous nodular structures in calcimudstone-wackestone facies. The field binder for scale is 30 cm long. (c) Elongated ferruginous nodules. Hammer is 32.5 cm long.

and Palma, 2009). Intercalations of massive sandstone (Sm) and black, laminated, bituminous shale (Fh) (Fig. 9c) support the interpretation that this sector of the ramp was sporadically affected by storms. Compared to the distal outer ramp, in this facies association there was a larger input of terrigenous sediments, more accentuated erosional features, and reworking by oscillating as well as unidirectional flows. The storm events transported parautochthonous-allochthonous organisms in suspension plumes eroded from shallower areas (probably from the photic zone where suspensivorous organisms dominated), which is consistent with the high-energy character of ammonite accumulations previously identified by Patarroyo (2009) in other parts of the basin. This also allowed the establishment of an opportunistic benthic community in an unstable, physically controlled environment as suggested by the presence of *Skolithos* isp. (Pemberton and MacEachern, 1997; Buatois and Mángano, 2011).

4.1.4. Facies association 4: proximal middle ramp

This facies association is arranged in tabular beds of 20–50 cm thick, dominated by medium-gray to black, massive to laminated, calcareous and siliceous siltstones (Slmc) with hummocky cross-stratification (HCS; Fig. 5d), massive to bioturbated calcimudstone-wackestone (Mm-Wm, Mm_b-Wm_b) (Fig. 7c), bioturbated wackestone (Wm_b) with remnants of HCS (Fig. 5c), and dm-thick, medium-gray, massive, sandy to bioclastic packstone (Pm) with normally sharp upper and lower contacts, although the latter may be occasionally erosional and reach up to 2 m where it is more sand-rich. The faunal content includes vertically stacked parautochthonous-allochthonous bivalves and crinoids that are generally disarticulated and highly fragmented, but the bioclasts in the Pm facies are coarser (>2 mm in mean diameter) and less well sorted compared to bioclasts in the Wm (<2 mm mean diameter) facies. They are also are less rounded, and more oblique to perpendicular to the bedding planes. The latter facies is vertically associated in rhythmic sequences (Fig. 9a), starting with massive packstone (Pm) that occasionally displays a crude fining-upward trend in bioclasts, followed by massive wackestone-calcimudstone (Wm-Mm), sometimes bioturbated wackestone (Wm_b) with remnants of HCS (Fig. 5c), and calcareous, bioturbated siltstones (Smlc) with HCS (Fig. 5d), grading into sandy mudstone at the top. Some intercalations of massive bituminous marlstones (Mrm), massive sandstone facies (Sm) with a lenticular to tabular geometry, occasionally inversely graded with wavy and ripple lamination (Swr), and inversely graded packstone (Pmg) are also present. The calcimudstone and wackestone show mottled structures (Fig. 7c), but single trace fossils cannot be recognized. This association of facies is dominant in the Rosablanca Formation and subordinate in the Paja Formation.

These rhythmic sequences (Fig. 9a) are interpreted as having been generated by turbulent (both oscillatory and unidirectional) flows in an open marine, middle ramp environment above the storm wave base. The grain-supported texture dominated by allochthonous bioclasts indicates deposition in a high-energy ramp domain. The parautochthonous fraction in mud-supported textures with intense bioturbation in the upper segments of the overall fining-upward sequence represents deposition during the waning phases of storm-triggered flows (Bádenas and Aurell, 2001; Martini et al., 2007). On the other hand, coarsening-upward beds and stacked bivalves indicate an increase in bottom friction as is typical of debris flows and traction carpets (Spalletti et al., 2000; Kietzmann and Palma, 2009). Despite the occasional traction structures in sandstone (Swr) and coarse bioclastic fraction in the Pm facies, this facies association was not formed on the inner ramp, but in the most proximal area of the middle ramp (indicated by 4,

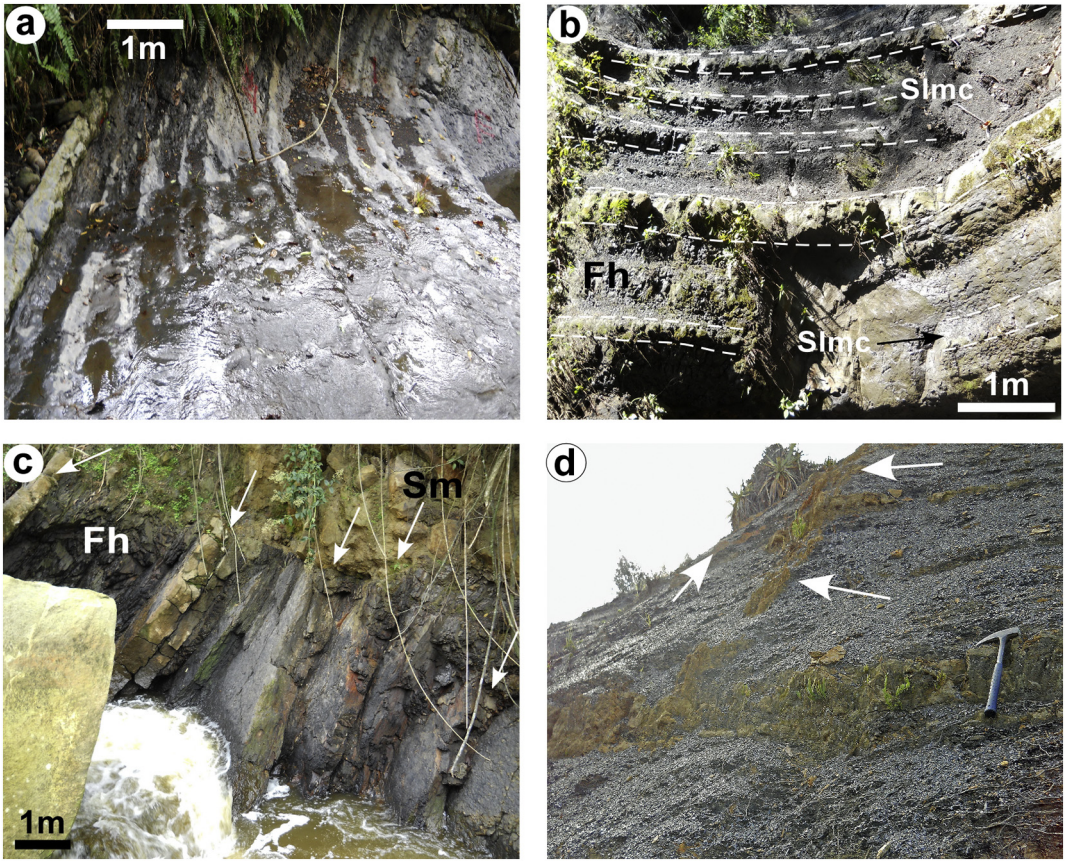

Fig. 9. Outcrop features reflecting storm processes and silt/sand injectites in response to the migration of fluids. (a) Proximal tempestites in the Rosablanca Formation (QLB section). (b) (c) Distal tempestites related to diluted turbidity currents, developed in the upper Paja Formation (b) and Simití Formation (c). Note intercalations of facies Smlc2, Sm with facies Fh. (d) Clastic injectite structures (indicated by white arrows) in black shales of the Simijaca Formation (CSR section).

in Fig. 10). This environment was characterized by moderate to high energy generated by storm-induced waves and oscillatory currents with better oxygenated conditions and minor deposition from suspension, both favourable for the establishment of an opportunistic benthic community.

4.1.5. Facies association 5: distal shallow inner ramp

This is the highest energy facies association encountered in the present study. It is composed of sub-tabular, sharp based, massive packstone with inverse grading of the bioclasts (>2 mm in mean diameter) (Pmg) and bioturbated, calcareous fine-grained sandstones with remnants of wavy lamination (Sm_b, Swr) showing a tabular geometry with sharp, low-relief erosional contacts. There are also, tabular, coarse bioclastic, sandy grainstone with some isolated current ripples (Gbr) intercalated with lenticular to tabular, calcareous sandstones showing current ripple cross-stratification (Fig. 5b) and wavy lamination (Swr). The latter have sharp, erosional contacts at the base and undulate contacts at the top. Amalgamated beds of massive, calcareous, fine-grained sandstones with shell lag deposits (Sm, Sm_f) showing slightly undulate, erosive bases, interbedded with black, laminated, bituminous shale (Fh) are also present. The thickness of the sandstone beds ranges from 0.5 m up to 2 m, whereas the packstone and grainstone are up to 1 m thick. The fossils are moderately fragmented and disarticulated, with signs of abrasion, and a generally chaotic orientation but sometimes oblique or perpendicular to the bedding. They include an autochthonous assemblage of crinoids, bivalves, and oysters (Fig. 6e), while scarce and small bryozoans and echinoderms are also present. Although some evidence of bioturbation was observed, single trace fossils cannot be recognized. This facies association is only present in the Paja Formation, where it is subordinate.

Facies association 5 represents deposition in warm, well oxygenated water with normal salinity, which provides the ideal condition for crinoids (Martini et al., 2007). The normal gradation, fragmentation, articulation, and distribution of bioclasts suggest storm-generated, unidirectional, turbulent flows (Spalletti et al., 2000; Kietzmann et al., 2008, 2014; Kietzmann and Palma, 2009), although the semi-vertical orientation of some clasts also indicates wave action. The abrasion observed in the bioclasts suggests a high-energy environment subject to frequent wave action above the fair-weather wave base. This is supported by traction structures in sandstones (Swr) and grainstones (Gbr). However, the bioturbation in some sandstone beds and the intercalation of black, laminated shale (Fh), suggest deposition in more tranquil conditions, probably triggered by oscillation of the relative sea-level (i.e., short transgressive pulses). The absence of well-developed planar cross-stratification does not allow us to interpret this facies association as typical of carbonate shoals that developed close to the shoreline, but the ripple cross-stratification (Fig. 5b) and wavy lamination in sandstones and grainstones, suggest wave action combined with bottom currents that continuously reworked the sediments transported during storms to distal parts of the inner ramp (Spalletti et al., 2000; Bádenas and Aurell, 2010). Therefore, we interpret this facies association as reflecting storm-generated sands and carbonate sheets or shoals of low relief in the distal, shallow inner ramp (indicated by 6, in Fig. 10).

4.2. Depositional model

The studied Cretaceous succession shows a gradual transition from shallow to deeper marine facies, without evidence of large-scale slump structures that would indicate a continental slope environment. There are also no facies related to reefs or calcareous mounds that would suggest a reef-rimmed shelf, so that deposition probably occurred on very gently sloping (<0.3°), stacked, homoclinal ramps (Figs. 10 and 15).

The ramp model was subdivided into five different sub-environments (Fig. 10) as discussed above, based on bathymetric criteria, sedimentary structures and derived energy conditions. However, according to the classification of Read (1985), our shallowest marine facies (distal shoal-water complex) of the inner ramp can be associated to barrier-bank complexes characterized by skeletal carbonate or sandy shoals suggesting a humid rather than arid climate, which would have prevented hypersaline conditions. This warm and humid climate during the Cretaceous in Colombia (Villamil, 1998) most likely exerted a strong control on the nearby sediment source areas (e.g., Santander-Floresta palaeomassif) and could explain the large amounts of nutrients in surface waters (see Section 4.3).

The dominant processes on homoclinal ramps are similar to those of siliciclastic shelves, in which the main mechanism of sedimentation and transport is related to storms (Fig. 9a, b, and c). The studied facies reflect storm action from the inner ramp to the distal basin, with limited evidence for normal wave or tidal action. This is coherent with the processes that generally dominate ramps in epicontinental seas, where tides and waves are attenuated by constant friction over a shallow, extensive sea bottom (Tucker and Wright, 1990). This domination by

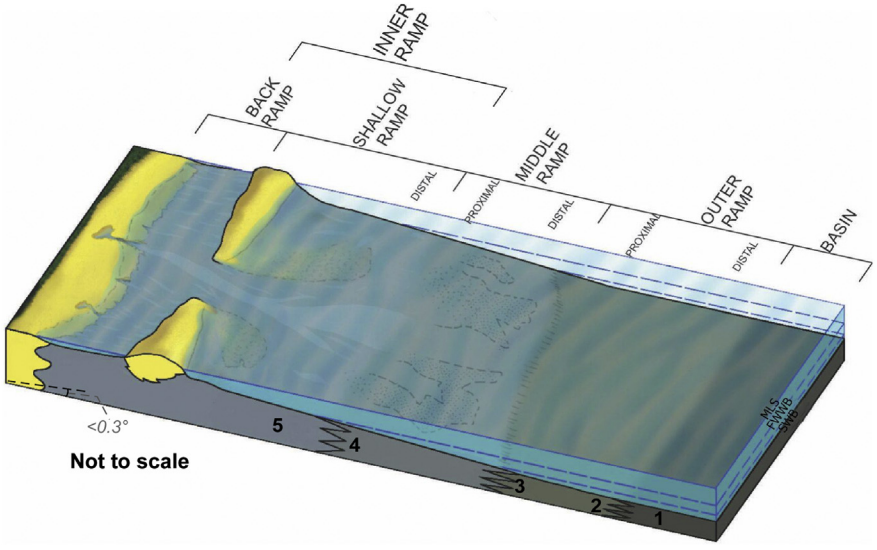

Fig. 10. Depositional model with facies associations indicated by numbers. Note storm-generated bioclastic shoals in the distal, shallow inner ramp domain and submarine channels enhanced by the strong influence of storm currents. MLS = mean sea level; FWWB = fair-weather wave base; SWB = storm wave base.

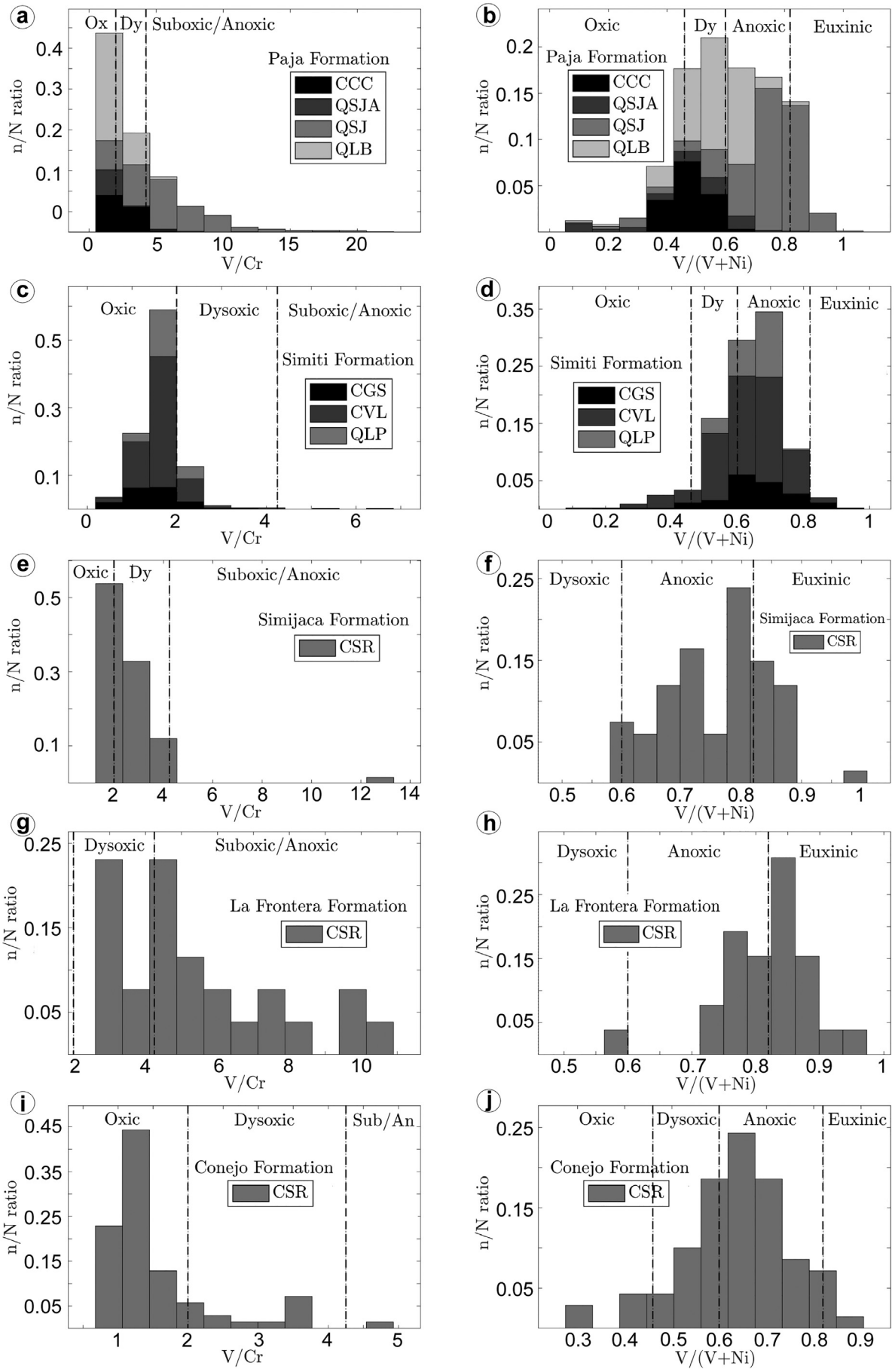
a
Ox
Dy
Suboxic/Anoxic
Paja Formation
CCC
QSJA
QSJ
QLB
n/N ratio
V/Cr
b
Oxic
Dy
Anoxic
Euxinic
Paja Formation
CCC
QSJA
QSJ
QLB
n/N ratio
V/(V+Ni)
c
Oxic
Dysoxic
Suboxic/Anoxic
Simiti Formation
CGS
CVL
QLP
n/N ratio
V/Cr
d
Oxic
Dy
Anoxic
Euxinic
Simiti Formation
CGS
CVL
QLP
n/N ratio
V/(V+Ni)
e
Oxic
Dy
Suboxic/Anoxic
Simijaca Formation
CSR
n/N ratio
V/Cr
f
Dysoxic
Anoxic
Euxinic
Simijaca Formation
CSR
n/N ratio
V/(V+Ni)
g
Dysoxic
Suboxic/Anoxic
La Frontera Formation
CSR
n/N ratio
V/Cr
h
Dysoxic
Anoxic
Euxinic
La Frontera Formation
CSR
n/N ratio
V/(V+Ni)
i
Oxic
Dysoxic
Sub/An
Conejo Formation
CSR
n/N ratio
V/Cr
j
Oxic
Dysoxic
Anoxic
Euxinic
Conejo Formation
CSR
n/N ratio
V/(V+Ni)

storm processes lasted from at least the Valanginian - early Hauterivian until the Albian, encompassing part of the Rosablanca Formation and most of the Simití Formation. Terraza (2012) also reported storm-related sedimentary processes during the Cenomanian when the Areniscas de Chiquinquirá Formation was deposited. During the Turonian-early Coniacian interval, although storm-related sedimentation took place on the outer ramp and basin of the Simijaca, La Frontera and part of the Conejo Formations, ocean bottom currents also played a role in the depositional system.

Recurring storm processes such as wind forcing and storm ebb-surge events provided an efficient mechanism to transport large amounts of circa-littoral, siliciclastic sediments and carbonate mud to deeper water in which black shales dominated. This allowed punctuated mixing, which gave rise to a mixed siliciclastic carbonate ramp. Thus, high-intensity clastic sedimentation frequently interrupted the general low-energy conditions, transferring material eroded from sandy and skeletal carbonate banks in the circalittoral zone to the middle and outer ramp in suspension plumes depositing proximal to distal tempestites. These higher-energy events allowed the deposition of mixed facies and probably favoured oxygenation in otherwise anoxic environments.

The marked absence of ichnofossils or bioturbation, together with the scarcity of autochthonous fossils in the fine-grained deposits of the distal outer ramp can be explained by the fact that trace-makers cannot establish themselves in highly saturated substrates under anoxic conditions. However, the presence of *Inoceramus* sp. in life position together with other small bivalves (Anomiidae?) indicates that there were also dysoxic pulses (Villamil, 1996) caused by disruptive distal tempestite deposition or weak bottom flow currents (Villamil, 1996; Rivera et al., 2016; this work). This allowed the adaptation of these organisms to oxygen-deficient conditions.

In the proximal outer ramp (Fig. 10) where loose substrates with relatively high oxygenation dominated, the trace fossil assemblage is represented by *Palaeophycus* isp., *Taenidium* isp., *Thalassinoides* isp., and *Planolites* isp. belonging to the *Cruziana* ichnofacies. The proximal *Cruziana* ichnofacies shows a higher diversity and abundance, suggesting the development of even softer substrates with high oxygenation but medium to high energy conditions in the proximal middle ramp. On the inner ramp, however, only isolated traces likely belonging to the proximal *Cruziana* or *Skolithos* ichnofacies are found, due to the fact that energy conditions were very high and the sedimentation of calcareous sandstones was rapid, which did not favour the diversity of trace-maker organisms.

With respect to the palaeogeographic context, the orientation and position of the coastline were very variable throughout the studied Cretaceous succession, which is also consistent with the early interpretations of Etayo et al. (1976). The shoreline also was controlled by the slope direction of the homoclinal ramps, which can be inferred by the palaeocurrent direction of ripple marks in the sandstone facies of the basal Paja Formation (Section 2: QSJ) that indicates a dominantly SSW trend (210°), and thus reflects an approximately E-W coastline orientation. This is supported by the fact that, within the whole succession of the ramp, the inner ramp facies has only been encountered in Section 2 (QSJ, Table 1) and not further towards the south in Section 3 (QLB, Table 1). The facies of the Paja Formation in Section 3, in fact, reflect a deepening of the ocean floor and increasing distance from the palaeo-coastline.

The southerly slope direction of the ramps lasted at least until deposition of the Simití Formation (Fig. 1). According to Moreno and Sarmiento (2002), there is a north to south increase in thickness towards the depocenter of the sub-basin. On the other hand, Terraza (2012), 40 km south of Barbosa (Fig. 2), reported the palaeocoastline to have been oriented close to N-S with a slope towards the west during deposition of the Areniscas de Chiquinquirá Formation (Fig. 1), which probably lasted until the deposition of the Simijaca, La Frontera and Conejo Formations (Section 7, CSR).

4.3. Evaluating the palaeoredox conditions

The assessment of palaeoredox conditions was performed only on the black shale succession (i.e., Paja, Simití, Simijaca, La Frontera and Conejo Formations). For the Paja and Simití Formations, we subdivided them into different sections instead of analyzing the entire formation. This approach allows us to evaluate variations in oxygenation in different parts of the basin. We also incorporated as a distinct class the arenaceous interval of the Paja Formation in Section 2, referred to as QSJA.

The Paja Formation in the CCC section (Section 1, Fig. 2 and Table 1) shows a domain of oxic-dysoxic conditions (Fig. 11a, b) with a mean value of 0.48 and 2.53 (dysoxic, Table 3) for the V/(V + Ni) and V/Cr ratios, respectively. Likewise, the arenaceous interval (QSJA) in the QSJ section (Section 2, Fig. 2 and Table 1) presents mean values of 0.46 and 2 (oxic, Table 3) for both ratios. However, for the ratio V/(V + Ni), wider oxygenation levels are observed, which range from oxic to anoxic, including a minimum proportion indicating euxinic conditions (Fig. 11a).

Poorer oxygenation conditions (dysoxic to euxinic; Fig. 11a, b) during sedimentation can be inferred for the rest of the Paja Formation in QSJ (V/(V + Ni) = 0.73 and V/Cr = 6.39; Table 3) and QLB (V/(V + Ni) = 0.56 and V/Cr = 2.28; Table 3). However, some differences can be observed depending on the ratio used, where for V/Cr the proportions of the dysoxic-oxic conditions are much more evident than for the V/(V + Ni) ratio in the case of the QSJ section (Section 2, Table 1) (Fig. 11a, b).

In all studied sections of the Simití Formation, there is not a good agreement between both environmental indicators (Fig. 11c, d). V/(V + Ni) indicates dysoxic to anoxic conditions while the V/Cr ratio suggests oxic conditions for most of the Simití Formation. In the QLP section (Section 4, Fig. 2 and Table 1), the V/(V + Ni) ratio (mean value of 0.65, Table 3) suggests a predominance of anoxic conditions but with some indications of better oxygenation levels, i.e., dysoxic (Fig. 11d). Although the V/Cr ratio presents a wider range of values, the level of dominant oxygenation is oxic, with a mean value corresponding to 1.7 (oxic, Table 3). On the other hand, for both the CVL section (Section 5, Fig. 2 and Table 1) and CGS sections (Section 6, Fig. 2 and Table 1) the V/(V + Ni) ratio shows a wide range of oxygenation, from oxic to euxinic, but with the highest proportions indicating anoxic conditions (Fig. 11d). The mean values correspond to 0.64 and 0.65 (anoxic, Table 3), in each section, respectively. However, for the V/Cr ratio, the variation is much more limited in both sections, the domain of oxic conditions dominating (Fig. 11c), with average values of 1.61 and 1.46 (oxic, Table 3) for both sections, respectively.

For the Simijaca, La Frontera and Conejo successions, an agreement between the relative levels of oxygenation can be observed from an independent analysis of each ratio and the integrated analysis of both. The V/(V + Ni) ratio indicates palaeoenvironmental conditions overwhelmingly in the anoxic to euxinic domain (Fig. 11f) in the Simijaca Formation (mean of 0.76, Table 3), which shifted to a lower oxygen regime during the accumulation of the La Frontera Formation (mean of 0.81, Table 3), but suggests less extreme conditions for the Conejo Formation (mean of 0.64, Table 3) with anoxic to dysoxic, and minimum euxinic and even oxic proportions (Fig. 11j). According to the V/Cr ratio, overall values are weighted towards more oxic conditions, correspondingly the

Fig. 11. Histogram showing palaeoredox proxies V/Cr and V/(V + Ni) for the studied black shale succession. Ranges for inferred palaeoxygenation conditions for V/Cr from Jones and Manning (1994) and for V/(V + Ni) from Hatch and Leventhal (1992). For location and names of sections see Fig. 2 and Table 1. N = total data of each formation; n = number of data in each palaeoxygenation range.

Table 3
Summary of selected trace element concentrations, redox-sensitive ratios and palaeoproductivity proxies of the Cretaceous black shales studied in comparison to the average shale, C/T mean black shales and average upper crust abundance.

Element/ratio	Avg. shale (μg/g)[a]	Avg. UCC (μg/g)[b]	Paja Fm. QSJ Section				Arenaceous member of Paja Fm. QSJA				Paja Fm. QLB Section			
			Min.	Mean	Max.	Std. dev.	Min.	Mean	Max.	Std. dev.	Min.	Mean	Max.	Std. dev.
Ti	4675.98	2457.89	90.60	2977.94	7231.13	1547.65	358.76	3329.38	7383.50	1973.99	262.37	4109.85	8692.21	1333.30
Cd	0.13	0.1	3.27	39.55	446.68	31.74	3.72	21.20	44.88	8.71	3.48	16.85	46.54	7.18
Ba	580	550	97.36	543.79	3555.03	182.05	76.28	542.41	757.95	99.39	119.26	637.8	881.98	93.00
Zn	95	71	17.86	783.54	12,849.16	1001.89	9.60	437.45	26,141.35	3140.92	21.87	75.3	1360.29	102.15
Cu	45	25	4.34	42.27	163.61	20.53	5.69	19.86	54.88	8.45	5.20	15.7	50.37	6.96
Ni	68	44	14.03	152.39	946.29	96.05	9.26	66.54	110.09	23.18	27.58	82.34	171.22	20.47
V	130	107	3.83	510.62	2360.34	347.55	4.98	65.18	174.72	41.44	6.44	109.67	399.15	42.80
Cr	90	83	3.19	96.12	273.06	48.09	3.46	39.91	103.79	26.35	3.65	53.08	118.25	20.56
Fe	48,261.87	24,480.66	731.05	20,747.15	399,298.59	26,347.67	3709.18	27,592.95	449,584.97	54,023.92	3108.54	24,393.14	92,219.16	8490.66
Mn	850	600	16.07	235.74	4843.18	319.18	70.39	392.00	2158.99	350.63	114.87	320.95	1225.32	162.46
Mo	1	1.5	2.12	122.87	1081.53	135.90	1.39	6.65	19.39	3.88	1.35	9.75	93.21	12.24
U	3.7	2.8	2.26	11.22	102.89	8.35	1.67	3.29	10.93	2.02	2.04	5.29	20.41	3.79
V/(V + Ni)	0.66	0.71	0.07	0.73	0.98	0.14	0.05	0.46	0.88	0.20	0.07	0.56	0.83	0.10
V/Cr	1.44	1.29	1.20	6.39	65.24	5.71	0.48	2.00	8.38	1.48	0.97	2.28	18.00	1.45
(Fe + Mn)/Ti	10.50	10.20	0.95	9.65	135.20	13.18	1.52	16.56	472.70	56.81	1.66	6.77	60.59	4.46

Trace elements concentrations in Cretaceous black shales of this study in μg/g; — represents not data.
[a] Average Shale data from Wedepohl (1971, 1991).
[b] Average Upper Crust Concentration data from McLennan (2001).
[c] Average Cenomanian-Turonian Black Shales data from Brumsack (2006).

Table 3 (*continued*)

Element/ratio	Paja Fm. CCC Section				Simití Fm. QLP Section				Simití Fm. CVL Section				Simití Fm. CGS Section	
	Min.	Mean	Max.	Std. dev.	Min.	Mean	Max.	Std. dev.	Min.	Mean	Max.	Std. dev.	Min.	Mean
Ti	1521.38	3306.02	5989.16	865.39	2905.56	7121.40	9733.08	1205.32	522.94	5803.26	8944.09	1668.06	2153.56	6219.71
Cd	8.92	18.25	39.66	5.53	3.40	10.81	26.57	5.60	3.43	12.80	32.94	7.00	3.52	10
Ba	432.82	693.23	991.71	69.45	13.94	502.6	765.88	86.72	363.62	559.14	915.10	88.57	232.33	476.6
Zn	29.58	66.67	1200.71	113.89	36.18	93.61	197.68	26.41	14.13	54.69	362.21	39.03	8.14	78
Cu	6.06	22.51	40.98	6.18	4.88	14.6	31.64	6.21	–	–	–	–	–	–
Ni	39.06	88.44	134.72	16.99	47.45	79.74	124.52	15.92	10.26	64.12	146.21	24.03	21.23	65.43
V	38.91	82.61	164.31	24.26	77.94	152.08	309.62	38.91	6.39	117.49	252.93	43.19	18.93	131.33
Cr	5.35	36.97	90.80	18.03	56.80	90.04	157.23	15.42	4.39	73.00	125.77	20.42	23.64	88.32
Fe	14,308.02	24,628.62	63,331.89	7201.21	8824.77	26,773.64	51,711.18	7801.09	3404.47	25,071.12	88,408.45	14,854.84	2221.97	29,390.00
Mn	165.63	479.61	2097.62	272.27	102.96	298.97	1114.81	183.71	72.23	269.18	2396.41	343.86	52.33	257.27
Mo	–	–	–	–	1.34	4.47	39.54	5.19	–	–	–	–	1.43	5.02
U	–	–	–	–	2.23	5.67	12.12	2.76	1.90	5.99	15.77	3.34	–	–
V/(V + Ni)	0.34	0.48	0.63	0.06	0.50	0.65	0.78	0.06	0.08	0.64	0.88	0.12	0.35	0.65
V/Cr	1.23	2.53	11.11	1.01	0.50	1.70	3.10	0.34	0.47	1.61	4.17	0.46	0.50	1.46
(Fe + Mn)/Ti	4.36	7.81	17.27	1.87	1.02	3.94	10.41	1.43	0.48	5.09	31.13	4.19	0.77	5.12

Table 3 (*continued*)

Element/ratio	Simití Fm. CGS Section		Simijaca Fm. CSR Section				C/T mean (μg/g)[c]	La Frontera Fm. CSR Section				Conejo Fm. CSR Section			
	Max.	Std. dev.	Min.	Mean	Max.	Std. dev.		Min.	Mean	Max.	Std. dev.	Min.	Mean	Max.	Std. dev.
Ti	12,183.52	1911.83	2367.67	4922.82	7366.71	1074.12	2697.68	627.99	2750.83	5567.92	1141.86	1068.58	3333.12	8201.17	1555.02
Cd	28.89	6.77	3.39	8.31	30.79	5.52	20.8	3.53	17.1	45.21	9.74	3.38	15.5	44.56	9.18
Ba	655.05	86.39	254.95	403.9	578.75	62.88	895	352.41	438.5	782.45	101.54	223.14	503.5	1279.89	187.57
Zn	1972.82	223.63	15.39	38.9	316.82	39.02	2056	7.60	118.5	746.30	185.73	7.61	68.2	945.76	157.10
Cu	–	–	–	–	–	–	194	–	–	–	–	–	–	–	–
Ni	117.32	21.42	8.36	57.31	156.47	17.93	267	43.02	88.2	241.27	52.89	12.77	53.94	181.35	29.01
V	219.20	48.85	68.57	216.11	1291.33	158.86	1016	97.73	471.47	1435.21	362.92	36.92	97.59	278.65	42.97
Cr	149.47	25.17	45.19	80.03	113.58	16.30	179	31.55	80.74	197.74	37.36	27.85	68.25	122.69	22.38
Fe	95,131.40	16,586.60	2871.66	6623.28	30,184.96	3802.40	38,329.72	1567.56	14,843.61	105,054.98	23,795.71	1458.74	46,249.84	446,534.88	96,234.92
Mn	1051.18	152.96	43.81	91.26	139.53	18.08	557	19.47	85.25	171.62	28.29	35.32	124.41	846.94	129.92
Mo	39.89	4.81	–	–	–	–	316	1.16	21.12	75.78	22.98	–	–	–	–
U	–	–	2.30	8.40	14.80	3.29	28	2.09	8.70	14.66	3.43	–	–	–	–
V/(V + Ni)	0.87	0.08	0.58	0.76	0.97	0.09	0.79	0.56	0.81	0.94	0.08	0.42	0.64	0.85	0.10
V/Cr	2.56	0.34	1.25	2.58	12.23	1.39	5.68	2.60	5.31	10.14	2.31	0.68	1.55	4.54	0.83
(Fe + Mn)/Ti	17.73	3.31	0.67	1.45	6.44	0.99	14.41	0.63	8.62	96.24	19.34	0.65	21.88	331.26	54.36

Simijaca Formation shows dysoxic levels of oxygenation (mean of 2.58, Table 3), while the La Frontera Formation was apparently deposited under suboxic-anoxic conditions (mean of 5.31, Table 3) and the Conejo Formation under oxic conditions (mean of 1.55, Table 3) with some punctual intervals under dysoxic levels.

Molybdenum is concentrated in organic-rich sediments and may be considered as one of the best diagnostic trace elements to assess anoxic and more prevailing euxinic conditions at the sediment-water interface (Algeo and Maynard, 2004; Rimmer, 2004). Molybdenum levels observed in the black shales of the Paja Formation (QSJ section, Table 3) are considerably higher than those of the average shale (1 μg/g, Wedepohl, 1971, 1991), average upper crustal abundance (1.5 μg/g, McLennan, 2001) and in average black shales (10 μg/g, cf. Rimmer, 2004), which may indicate persistent anoxia. However, in the QLB section (Section 4, Fig. 2 and Table 1) and the arenaceous interval (QSJA) of the Paja Formation, the molybdenum concentration is higher than that of the average shale and the average upper crust, but does not exceed the average black shales value. The same can be observed in the Simití Formation (Table 3).

As the Simijaca and the La Frontera Formations represent the Cenomanian - Turonian boundary (Fig. 1) in the study area, it may be reasonable to compare molybdenum concentrations also with the mean Cenomanian/Turonian values (Brumsack, 2006). The molybdenum abundance far exceeds that of the average shale, upper crust, and average black shales, which indicates extended anoxia during sedimentation. However, in the Simijaca and the La Frontera Formations, Mo values are well below the mean of the Cenomanian/Turonian values (316 μg/g, Brumsack, 2006).

4.3.1. The potential role of hydrothermal sources in palaeoredox conditions

The tectonic framework of the Eastern Cordillera Basin (see Geological setting section), where there are conspicuous lateral facies and thickness changes as a consequence of differential subsidence of tectonic blocks controlled by *syn*-sedimentary normal faulting favours manifestations of massive stratiform sulfides of Pb, Zn and Fe in black shales (Sarmiento-Rojas, 2002; Sarmiento-Rojas et al., 2006). Hydrothermal sources can release large amounts of Mn and Fe, which in turn can, from their reduction cycle, influence the concentration of redox-sensitive elements (e.g., Ni, Cu, Zn, Co, Pb, V, Mo and Cr) in oxygen-deficient conditions (Tribovillard et al., 2006). This can increase the anoxic levels until euxinic conditions are reached at the site of deposition. In order to test the hypothesis of whether hydrothermal sources contributed significant amounts of elements to the system, we used the (Fe + Mn)/Ti ratio as an indicator to evaluate the hydrothermal influence on sedimentation.

The (Fe + Mn)/Ti ratio values of most of the black shale succession of the Paja, Simití, Simijaca and La Frontera Formations lie outside the range of hydrothermal influence (Table 3), suggesting that the intensity of hydrothermal activity in the study area was rather weak or that the terrigenous input was sufficiently high to avoid exceeding the threshold. Nevertheless, the arenaceous member of the Paja and the Conejo Formations shows values higher than 15, indicating hydrothermal influence (Table 3). On the other hand, Figs. 12 and 13 show some peaks of stronger hydrothermal intensity in the Paja, Simití, La Frontera and Conejo Formations, reaching maximum values of up to 135, 472, 31 and 331 (Table 3), for each formation, respectively. It can be problematic to associate these hydrothermal peaks with magmatic activity, as we cannot observe any linkage between the bentonite layers and anomalies of the (Fe + Mn)/Ti ratio in the Simijaca Formation. However, we cannot rule out this possibility. Tentatively, we can speculate that each hydrothermal peak is related to tectonic activity, where hydrothermal fluids rich in Pb, Zn, Cu, Ba and Fe circulated along synsedimentary normal faults in locations of greater lithospheric stretching (i.e., greater subsidence) (Fabre and Delaloye, 1983; Sarmiento-Rojas, 2002; Sarmiento-Rojas et al., 2006). This would agree with the high values of

thermal maturity reached in the kerogen of the Paja Formation close to the study area (Sarmiento-Rojas, 2011).

4.3.2. Effects of sedimentation processes on the benthic O_2 levels

Oxygen replenishment can occur after the development of reducing conditions when environmental conditions vary sharply (e.g., during turbidite or tempestite deposition) and may remobilize some redox-sensitive elements (Tribovillard et al., 2006). In Figs. 12 and 13, there is an overwhelming coincidence between the deposition of strata interpreted as the products of storm activity and prominent lows in the V/(V + Ni) and V/Cr ratios, indicating better oxygenated episodes. In such tempestite beds, large suspension loads reaching distal parts of the basin lead to the establishment of an opportunistic benthic community in an unstable, physically controlled and at least temporarily oxygenated environment, as suggested by the presence of bioturbation in some of these beds. Carbonate was also a major diluting factor in the extended anoxic depositional environment, affecting the concentrations of redox-sensitive elements (Fig. 12), where the depletion of the benthic O_2 levels was accentuated by the absence of calcium carbonate. The latter observation supports the hypothesis raised in which carbonate produced in shallow waters was transported/remobilized by storm currents and deposited as carbonate mud plumes in deeper parts of the basin.

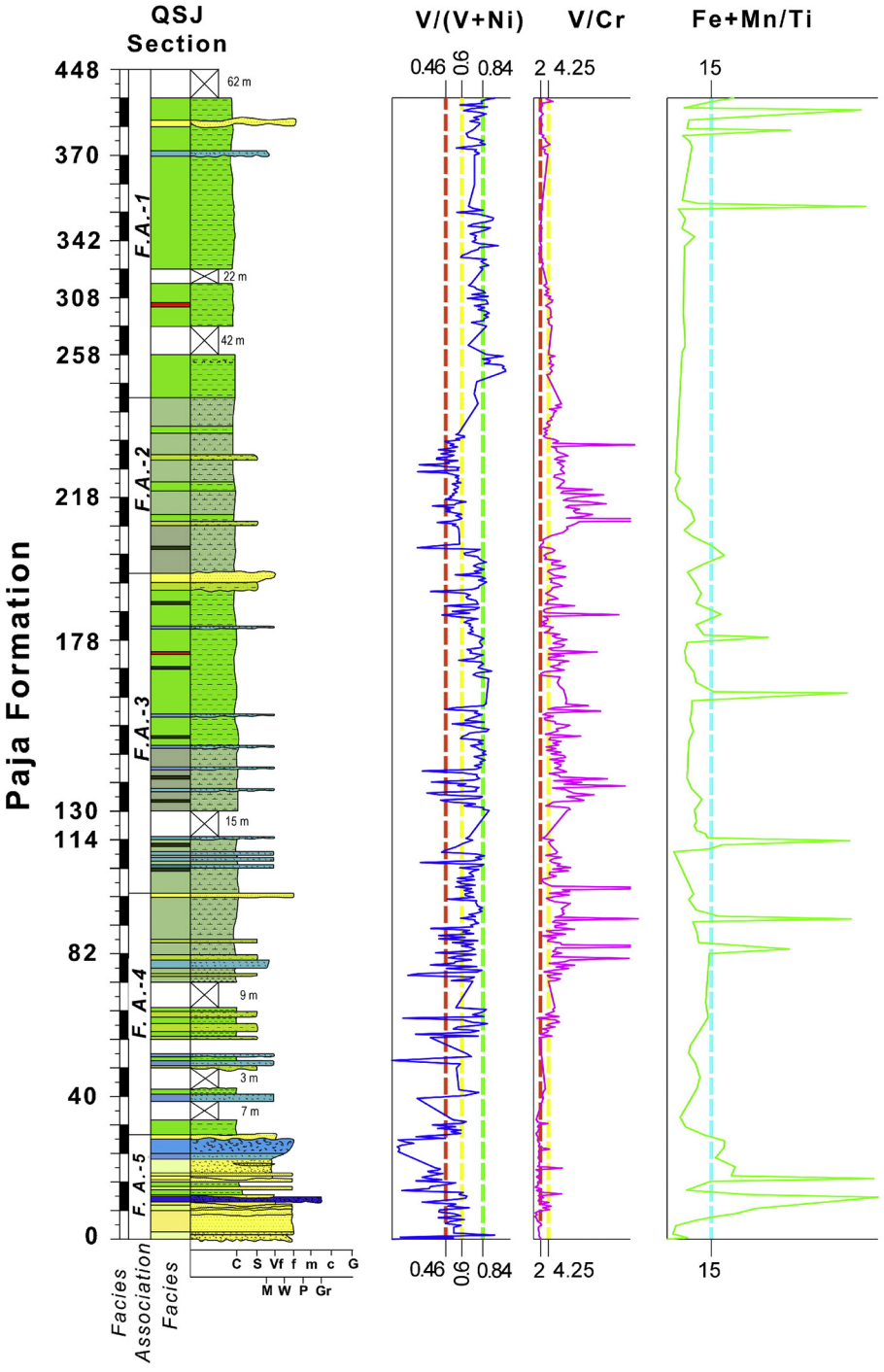

Fig. 12. A simplified stratigraphic column of the Paja Formation in Section 2 (see Fig. 2 and Table 1), showing redox-sensitive ratios V/Cr, V/(V + Ni) and hydrothermal activity ratio (Fe + Mn)/Ti. Note how tempestite beds interrupt continuum anoxic conditions.

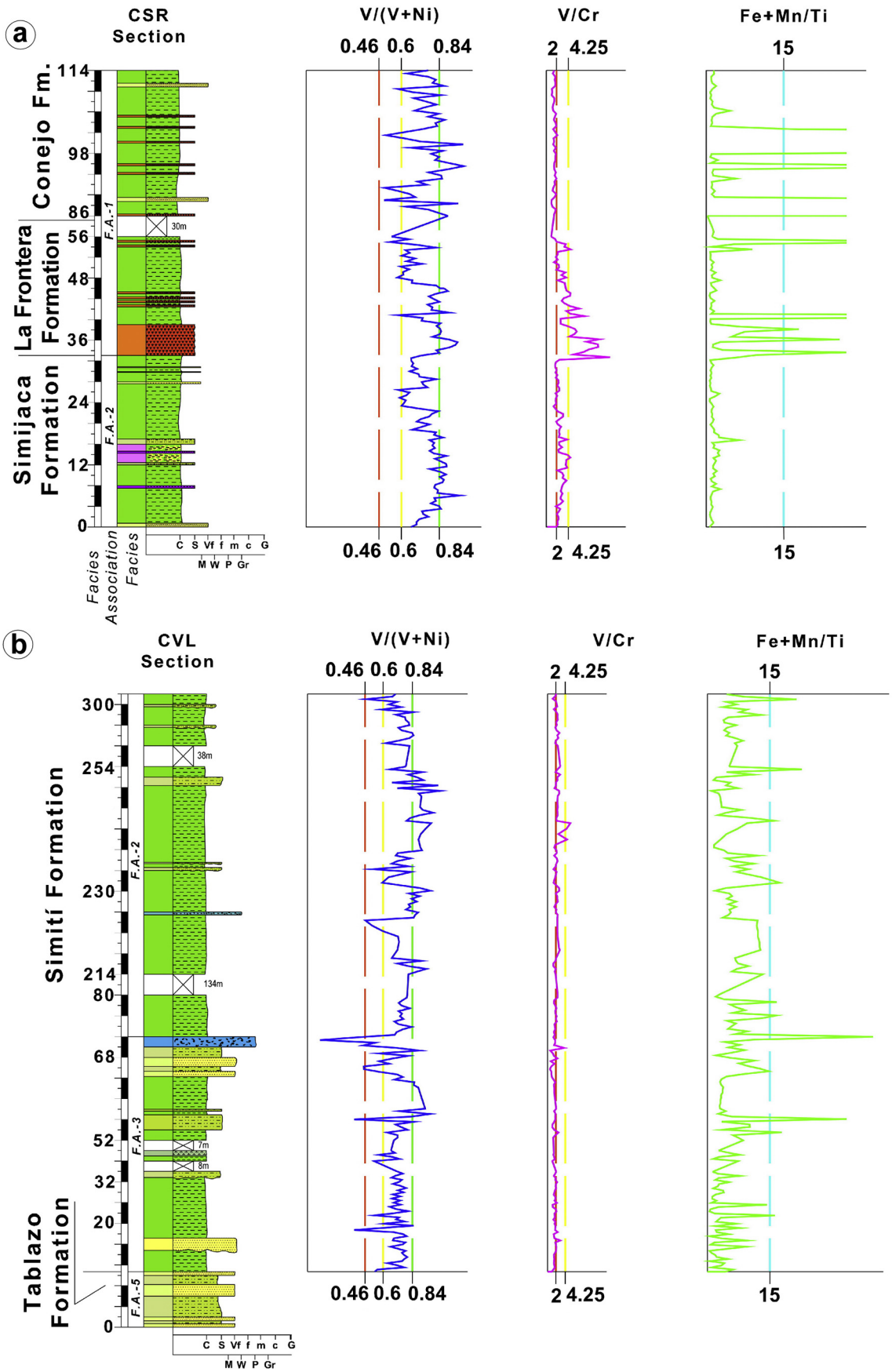

Fig. 13. Simplified stratigraphic columns of the Simití, Simijaca, La Frontera and Conejo Formations, showing redox-sensitive ratios V/Cr, V/(V + Ni) and hydrothermal activity ratio (Fe + Mn)/Ti. (a) Simijaca, La Frontera and Conejo Formations in Section 7 (see Fig. 2 and Table 1). (b) Simití Formation in section 5. Note how tempestite beds interrupt continuum anoxic conditions and strong correlation between peaks of hydrothermal activity and laminated chert (Lh) in La Frontera and Conejo Formations.

As suggested Tribovillard et al. (1991), episodic storm events and anoxic bottom water conditions are not incompatible, and this mechanism of sedimentation may have a dual behaviour, improving oxygenation conditions but also contributing to increased anoxia. After each storm event, sufficient continental organic detritus and/or nutrients may be supplied to surface waters by river discharge and storm currents, after which intense organic matter degradation can trigger anoxia (Tribovillard et al., 1991, 2006; Stow et al., 2001).

4.3.3. Origin of the organic matter and palaeoproductivity proxies

Fig. 14 shows the V/Ni ratios for the Paja, Simití, Simijaca, La Frontera and Conejo Formations, where the oxygenation ranges of the Paja and Simijaca Formations are consistent with the results obtained from the V/(V + Ni) and V/Cr ratios. For the Simití Formation, the oxygenation conditions during deposition are more constrained to oxic-dysoxic levels (Fig. 14b). However, for the La Frontera and Conejo Formations (Fig. 14c), benthic O_2 levels are opposite to those observed from the former proxies (Fig. 11), whose results show the most extreme conditions of palaeoxygenation during deposition of the La Frontera Formation and better benthic O_2 levels during deposition of the Conejo Formation.

The origin of the organic matter may be divided into two main groups: a predominantly a mixed terrestrial and marine origin for the Paja and Simití Formations (Fig. 14a, b), representing the Lower Cretaceous, and mainly marine for the Simijaca, La Frontera and Conejo Formations (Fig. 14c) corresponding to the Upper Cretaceous. This origin of the organic matter is consistent with a type II kerogen (marine) deposited in anoxic or oxygenated environments in the Upper Cretaceous source rocks in the Eastern Cordillera Basin and a type III kerogen (paralic marine) together with mixed type II/III kerogen, suggesting a higher proportion of plant organic-matter deposited in a marginal siliciclastic environment under better-oxygenated conditions for the Lower Cretaceous source rocks (Sarmiento-Rojas, 2011). Moreover, previous studies based on conventional petrographic analysis, advanced scanning electron microscope techniques and organic geochemistry, have evidenced a large supply of terrigenous components and nutrients in deeper shelf environments sourced from the mainland (Mann 1995 cf. Gaona-Narváez et al., 2013; Gaona-Narváez et al., 2013) during sedimentation of the Paja Formation. There was also a high input of authigenic quartz of biogenic origin in time-equivalent rocks of the Simijaca and La Frontera Formations in the Eastern Cordillera Basin, sourced by high marine productivity (Buckman et al., 2017).

Despite the complications to obtain a quantitative proxy of primary palaeoproductivity in ancient environments, it may be possible to achieve a relative estimation of the variation of productivity rates based on trace metal proxies such as Zn, Ni, Cu, Cd, Cr and Ba (Tribovillard et al., 2006; Brumsack, 2006; Goldberg and Humayun, 2016), although the use of Ba as a palaeoproductivity marker in black shales is rather problematic (Tribovillard et al., 2006; Brumsack, 2006). Based on the average of all the lithostratigraphic units studied, Cu, Cr and Ba are depleted in comparison to the average shale (Table 3), although Zn, Ni and Cd show enrichment for the Paja, Simití and La Frontera Formations. However, when the Simijaca and the La Frontera Formations are compared to the average Cenomanian/Turonian rocks, they appear to be depleted (Table 3). The enrichment of Zn, Ni, and Cd in the La Frontera Formation may explain the silicification within these strata in response to the remobilization of biogenic silica favoured by high marine palaeoproductivity related to upwelling processes, which is consistent with the model proposed by Macellari and De Vries (1987), Tribovillard et al. (1991), Villamil (1996) and Villamil and Arango (1998) to explain the high amount of organic matter in the Upper Cretaceous units. The latter authors proposed a high marine productivity and accumulation of silica of organic origin driven by vigorous upwelling at the Cenomanian/Turonian boundary, which in turn, caused accumulation of large amounts of organic matter and subsequent expansion of the oxygen minimum zone favouring the preservation of organic matter and enrichment in sediments. Thus,

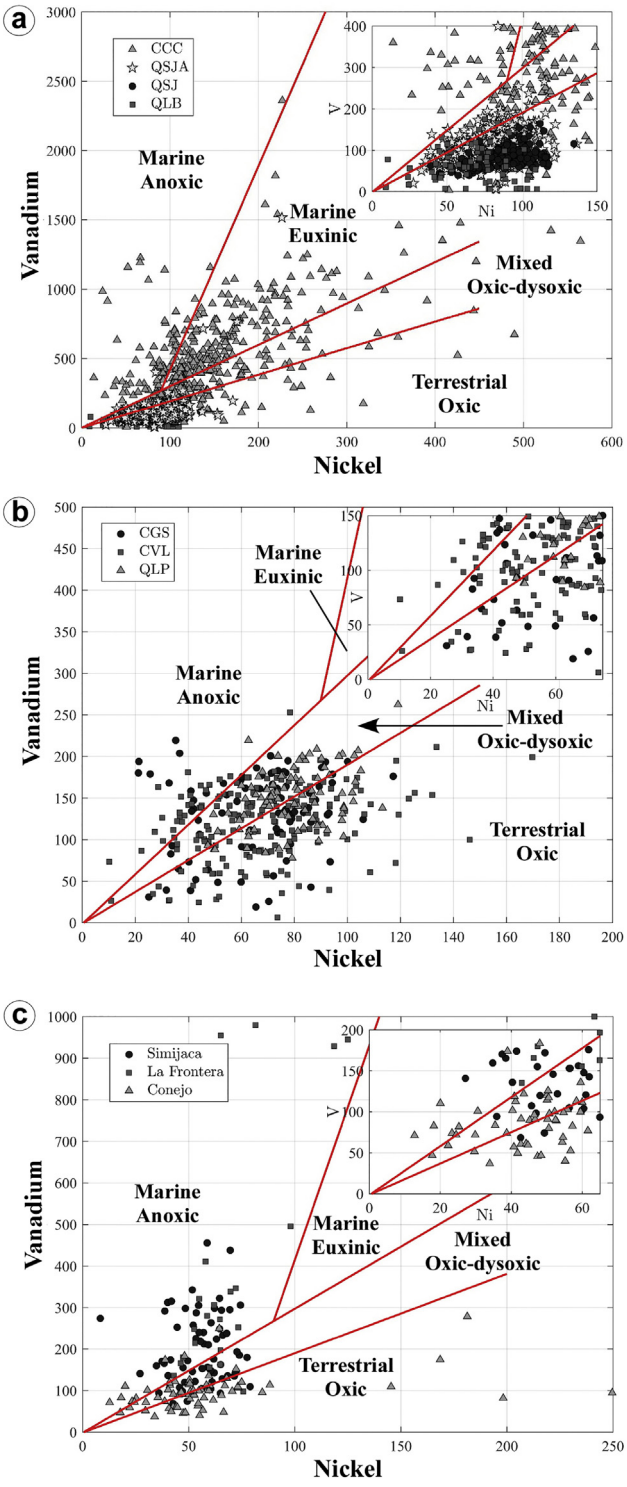

Fig. 14. Crossplot of V vs. Ni concentration in μg/g for each formation studied. (a) Samples of the Paja Formation in each section studied (see Fig. 2 and Table 1). Note: QSJA represents the arenaceous interval of the Paja Formation. (b) Samples of Simití Formation in each section studied (see Fig. 2 and Table 1). (c) Samples of the Simijaca, La Frontera and Conejo Formation in Section 7 (see Fig. 2 and Table 1). The range for inferred organic matter origin and palaeoredox conditions from Galarraga et al. (2008).

according to the upwelling system model, the anoxic sedimentation responds to a regional anoxic event rather than a global anoxic event.

On the other hand, for the Lower Cretaceous interval, i.e., the Paja and Simití Formations, relatively few studies have tackled their enhanced preservation of organic matter and causes of depleted benthic

oxygenation. Gaona-Narváez et al. (2013), based on stable carbon isotopes, TOC, and palaeontological data, determined that the prevailing anoxic organic-rich shales at the base of the Paja Formation are not related to global oceanic anoxic events, because the isotopic carbon excursion corresponding to the Aptian OAE-1a is absent from the stratigraphic record. Our results suggest that the high organic matter content in the Paja and Simití Formations may be a function of primary productivity produced mainly by continental runoff. Although the existence of authigenic pyrite and lack of bioturbation may be an indirect indicator of sluggish bottom waters, these features can also be related to oxygen depletion as a consequence of large amounts of oxidizing organic matter in a highly productive water column. Therefore, a productivity-anoxia feedback system may have developed, where a contemporaneous interplay between anoxic-euxinic and bio-productive conditions existed. Moreover, a warm and moist climate favours the accumulation of nutrients without the need of sluggish bottom water circulation that induces poor oxygenation levels (Meyer and Kump, 2008), as might have been the case in the Eastern Cordillera Basin.

4.4. Sequence stratigraphy

Sequence 1 corresponds entirely to the uppermost part of the Rosablanca Formation and includes a transgressive (TST-1) and highstand (HST-1) systems tract, well defined in Section 3 (QLB, Fig. 3). In Section 1 (CCC, Fig. 3), it was only possible to recognize the upper part of HST-1. TST-1 is composed of facies Mrl intercalated with facies Mmb-Wmb. The transgressive surface (TS) could not be identified within this section, as the TST-1 was here represented by the last stage of sedimentation before reaching the maximum flooding surface (MFS), characterized by dark marlstone with a high proportion of pyrite and organic material and the absence of fossils. These indicate anoxic-euxinic conditions typical of condensed sections. The first few meters of HST-1 is characterized by an aggradational pattern composed of facies Smlc, followed by a progradation pattern, likely related to a downlapping as interpreted in Fig. 15. The development of fourth/fifth order parasequences indicates a clear shallowing-upward trend represented by proximal tempestites of the facies Pm-Wm-Mm-Slmc (Fig. 9a). This sequence marks a progressive change from facies association 3 to facies association 4 during a sea-level stillstand, just before the next major fall in sea-level.

Sequence 2 almost includes the complete Paja Formation, being composed of the LST-2, TST-2 and HST-2 systems tracts that are well exposed in Section 2 (Fig. 3). In Section 3, only the last two tracts could be recognized, implying that the geographic location of this section was farther from the palaeocoastline (Fig. 15). The stratigraphic profile of the Paja Formation measured in Section 1 (CCC, Fig. 3), was not included in the sequence analysis, because of a faulted contact with the underlying Rosablanca Formation, which eliminated the basal part of the Paja Formation. The sequence boundary is associated with the erosional base of the first fossiliferous sandstone in Section 2, which most likely represents a subaerial unconformity. However, it was not possible to establish the relationship between LST-2 and its predecessor HST-1 from the limited outcrops in the study area, but the absence of karst, calcrete or major erosional surfaces, and only evidence of horizons exposed to wave erosion without subaerial deposits within facies association 5, suggest an episode of normal regression or a minor to third-order regressive pulse. LST-2 is characterized by facies Sm_f, Swr, Gbr, and Pm, with thin mudstone and sandy siltstone interbeds, indicating sporadic interconnection with fine sediments of the deeper ramp (Fig. 15). The TS is marked by a change to pyritic, well-laminated shales (Fh facies) initiating TST-2 in Section 2 (Fig. 3). In Section 3, due to its larger distance from the shore, facies Fh, with a high concentration of reworked fossils, is interpreted as transgressive lag deposits representing the TS and also the sequence boundary marking the start of sequence 2. TST-2 shows a retrogradational, onlap stacking pattern (Figs. 3 and 15), formed by successive fifth order parasequences in which each involves deeper water facies (Fh, Mrl, Mrm) and reduced participation of shallower water facies (Slmc, Swr) in ascending order. This reflects a progressive deepening of the sandstone lithosomes of LST-2 in conditions where the rise in sea-level had a greater influence than the carbonate production. The MFS marking the boundary between TST-2 and HST-2 is characterized by the development of concretion horizons (Fig. 8b), reflecting stratigraphic and sedimentological condensation (a decrease in thickness and progressive cementation in Section 3), but not taphonomic condensation. This can probably be explained by the anoxic-euxinic conditions in the water column that inhibited the colonization of benthic and even nektonic organisms. HST-2 is composed of facies Fh, Mrl, and Mrm, with frequent intercalations of slightly coarser facies Slmc, forming probably a less clear progradational stacking pattern (Fig. 15) than the systems tract of the previous sequence.

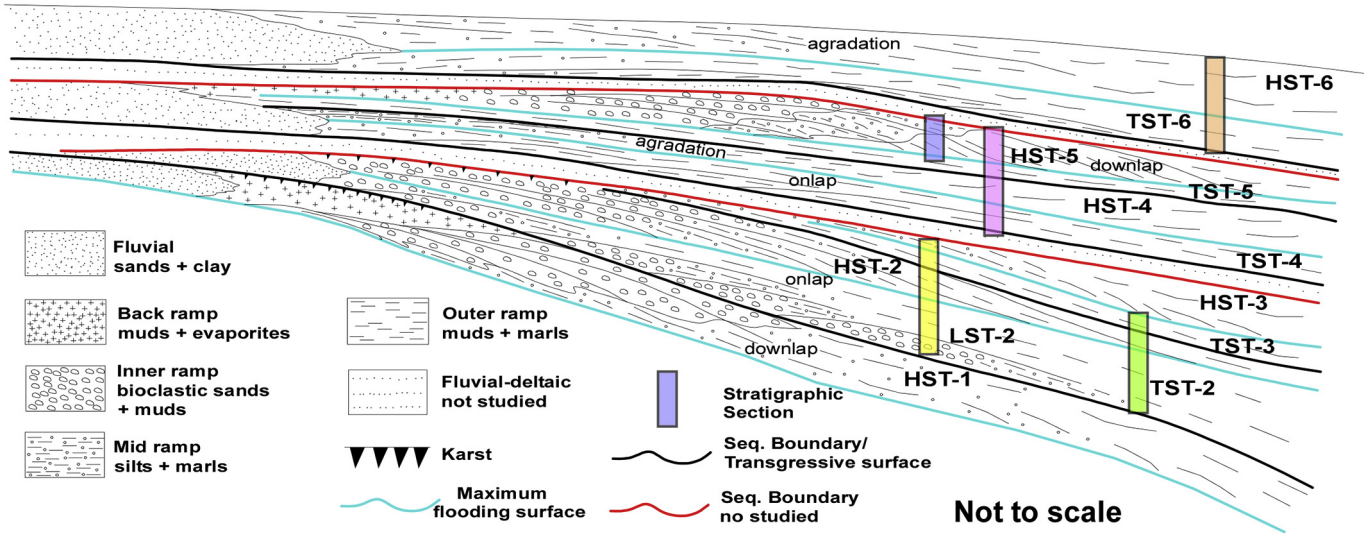

Fig. 15. Idealized sequence stratigraphic model of the Magdalena-Tablazo Sub-Basin from stratigraphic sections measured, showing sequence geometry, main stratigraphic surfaces, facies and inferred stacking patterns of each systems tract. Note that most of systems tracts correspond to deeper part of the basin for the studied Cretaceous succession. Yellow = QSJ section; Green = QLB section; Magenta = QLP section; Blue = CGS section; Orange = CSR section.

This indicates a more aggradational system and increased accommodation space, which was so much that the inner ramp facies belt (facies association 5) changed to deeper associations of the distal, outer ramp (facies association 2), without showing a clear regressive tendency as could have been expected.

Sequence 3 is recorded in the uppermost part of the Paja Formation and is constituted by the TST-3 and HST-3 systems tracts (Fig. 3), being fully identifiable in Section 2. In Section 3, only the latter tract can be recognized. The base of the sequence is located in the TS, thus representing a marked deepening and expansion of the basinal facies association 1 that characterize TST-3 above the outer ramp deposits of the previous sequence. This suggests that the ramp responded rapidly to small oscillations in the relative sea-level triggered by local tectonic effects. The MFS is represented by the development of concretion horizons and could only be identified in Section 2 (Fig. 3). HST-3 in the latter section is composed of facies Fh that intercalate upward in the succession with facies Mm-Wm and Swr. The poor development of parasequences in HST-3 does not allow a clear identification of the stacking pattern. However, it is interpreted to be progradational (Figs. 3 and 15) indicating the start of a regressive cycle that is clearly exhibited in the overlying Tablazo Formation. Although the latter was not studied in detail here, we did find evidence of a fall in relative sea-level, as indicated by desiccation cracks developed in microbial mats of a possibly supratidal environment (Fig. 5h). The latter agrees with observations of Guerrero et al. (2000), placing a sequence boundary close to the Aptian-Albian boundary (Fig. 1), related to shallowing of the environment in the transition of the Paja to Tablazo Formations (Moreno and Sarmiento, 2002).

Sequence 4 constitutes the major part of the Simití Formation and includes the TST-4 and HST-4 systems tracts. These can be identified mainly in Sections 4 and 5 (Fig. 4). The base of the sequence is located in the TS, which represents an abrupt deepening and expansion of the basin facies (Fh) that characterizes TST-4 above the lowstand deposits of the underlying Tablazo Formation. The MFS, characterized by marlstones and dark, organic shales (Fig. 5a) as well as an absence of fossils, indicates anoxic-euxinic conditions typical of condensed sections. These could be clearly recognized only in Section 4, as in Section 5 only the TST-4 systems tract could be identified. The MFS marks the commencement of HST-4, which is composed of facies Fh, normally characterized by vertical accretion with rapid sedimentation typical of aggradational stacking (Figs. 4 and 15).

Sequence 5 is an up to fourth order cycle, thus being of a lower hierarchy than underlying sequences. It coincides with the uppermost part of the Simití Formation in Section 6, where the TST-5 and HST-5 systems tracts (Fig. 4) could be recognized. The TS could not be identified, but it is inferred that the basinal facies association 1 represents TST-5. The latter has poorly developed parasequences, in contrast with HST-5 in which a progradational stacking pattern can be clearly recognized (Figs. 4 and 15). The latter is represented by coarsening- and thickening-upwards pattern in the succession. The rapid transition from one systems tract to the next is characteristic (Fig. 4), which is probably related to an acceleration in basin shallowing before the start of the LST that characterizes the Areniscas de Chiquinquirá Formation where Guerrero et al. (2000), Guerrero (2002) and Terraza (2012) placed a sequence boundary related to relatively fast sea-level fall at the base of Cenomanian strata (Fig. 1). Therefore, it is difficult to establish the MFS in this sequence, which was consequently assigned to the interval of major phosphate enrichment (Fig. 4).

Sequence 6 overlies the previously described depositional systems in Section 7, where the Cenomanian - Turonian limit (Fig. 1) corresponds to the most important TS of the Cretaceous (Villamil and Arango, 1998). Above this boundary lies the TST-6 systems tract (Fig. 4), represented by massive to laminated mudrocks and bentonites of the Simijaca Formation (Fh, Tm, Hlh). These facies characterize a restricted, distal, outer ramp association. The MFS is located around the 33 m mark of Section 7, at the base of silica-rich siltstones and cherts of the La Frontera Formation, where vertical accretion prevailed (Figs. 4 and 15). This initiated HST-6, which extends at least to the base of the Conejo Formation. These systems tracts are consistent with those interpreted by Villamil (1998) and Villamil and Arango (1998) in age-equivalent rocks in other parts of the Eastern Cordillera Basin and Middle Magdalena Basin.

5. Conclusions

A better understanding of sedimentary processes during deposition of the Cretaceous black shales in the Magdalena-Tablazo Sub-Basin allows an improved reconstruction of facies distributions and changes within the sub-basin, which reflect a mixed siliciclastic-carbonate homoclinal ramp (Figs. 10 and 15) dominated by storms. The latter were the driving mechanism of the mixed siliciclastic-carbonate nature of the ramp system.

The dominance of TST and HST over other systems tracts in the studied Cretaceous succession allows us to infer ample accommodation space and relatively low energy conditions on the ramp. This allowed the establishment of very low gradient depositional slopes (<0.3°) in response to major marine transgressions over long periods.

During sedimentation of the Paja, Simití, Simijaca, La Frontera and Conejo Formations the environment was mostly depleted in oxygen. However, episodic storm events allowed better oxygenation levels and the proliferation of benthic organisms.

The cause of the accumulation of the Cretaceous thick black shale succession in the Magdalena-Tablazo Sub-Basin is believed to correspond to high productivity in the water column causing a productivity-anoxia feedback system with a high biological oxygen demand. The latter supports the hypothesis of a regional high nutrient and primary productivity superimposed on the global anoxia events.

Preservation of the organic matter was also favoured by the faster rate of burial or subsidence recorded during the Cretaceous, which might have allowed a short time of exposition to oxidation or degradation by benthic fauna. Rises in sea-level and episodic hydrothermal input were also important mechanisms to enhance anoxic- to - euxinic bottom waters.

Acknowledgments

This research was part of the undergraduate thesis of H.A.R completed at the Universidad Pedagógica y Tecnológica de Colombia, supported by Gems S.A., whom the senior author is greatly indebted to for financial and logistical support. We acknowledge especially Cesar Mora and Alexander Piragüa for their constructive review during the undergraduate thesis preparation. Thanks to Nesyereb Suárez for her assistance in field work and Darío Lazo for his very kind and helpful assistance in *Trigonia* identification; also to Andres F. Salcedo who helped with some graphic preparations and to Xavier Emery for an early editing of the English. H.A.R. and J.P.L.R. also acknowledge logistical support from Projects FONDAP 15090013 and FONDECYT 1130006 in the preparation of this manuscript. We appreciate the thoughtful review of Dr. Diego Kietzmann and the Editor of Sedimentary Geology, Dr. Brian Jones, whose comments improved greatly the manuscript.

References

Algeo, T.J., Maynard, J.B., 2004. Trace-element behavior and redox facies in core shales of Upper Pennsylvanian Kansas-type cyclothems. Chemical Geology 206:289–318. https://doi.org/10.1016/j.chemgeo.2003.12.009.

Aurell, M., 1991. Identification of Systems Tracts in low angle carbonate ramps: examples from the Upper Jurassic of the Iberian Chain (Spain). Sedimentary Geology 73, 101–115.

Bádenas, B., Aurell, M., 2001. Proximal-distal facies relationship and Sedimentary processes in a storm dominated carbonate ramp (Kimmeridgian, northwest of the Iberian Ranges, Spain). Sedimentary Geology 139, 319–342.

Bádenas, B., Aurell, M., 2010. Facies models of a shallow-water carbonate ramp based on distribution of non-skeletal grains (Kimmeridgian, Spain). Facies 56, 89–110.

Brumsack, H.J., 2006. The trace metal content of recent organic carbon-rich sediments: implications for Cretaceous black shale formation. Palaeogeography, Palaeoclimatology, Palaeoecology 232:344–361. https://doi.org/10.1016/j.palaeo.2005.05.011.

Buatois, L., Mángano, M.G., 2011. Ichnology: Organism-Substrate Interaction in Space and Time. Cambridge University Press, Cambridge, UK, p. 347.

Buckman, J., Mahoney, C., März, C., Wagner, T., Blanco, V., 2017. Identifying biogenic silica: mudrock micro-fabric explored through charge contrast imaging. American Mineralogist 102:833–844. https://doi.org/10.2138/am-2017-5797.

Bürgl, H., 1967. The orogenesis of the Andean system of Colombia. Tectonophysics 4, 429–443.

Cardozo, E., Ramírez, C., 1985. Ambientes de depósito de la Formación Rosablanca: Área de Villa de Leyva, Chapter XIII. In: Etayo, F., Laverde-Montaño, F. (Eds.), Proyecto Cretácico, contribuciones. Publicaciones Geológicas Especiales-Ingeominas, Bogotá, p. 16 (13).

Catuneanu, O., Galloway, W.E., Kendall, C.G., Miall, A.D., Posamantier, H.W., Strasser, A., Tucker, M.E., 2011. Sequence stratigraphy: methodology and nomenclature. Newsletters on Stratigraphy 44:173–245. https://doi.org/10.1127/0078-0421/2011/0011.

Christ, N., Immenhauser, A., Wood, R.A., Darwich, K., Niedermayr, A., 2015. Petrography and environmental controls on the formation of Phanerozoic marine carbonate hardgrounds. Earth-Science Reviews 151:176–226. https://doi.org/10.1016/j.earscirev.2015.10.002.

Cobbold, P.R., Zanella, A., Rodrigues, N., LØseth, H., 2013. Bedding-parallel fibrous veins (beef and cone-in-cone): worldwide occurrence and possible significance in terms of fluid overpressure, hydrocarbon generation and mineralization. Marine and Petroleum Geology 43, 1–20.

Cooper, M.A., Addison, F.T., Álvarez, R., Coral, M., Graham, R.H., Hayward, A.B., Howe, S., Martínez, J., Naar, J., Peñas, R., Pulham, A.J., Taborda, A., 1995. Basin development and Tectonic history of the Llanos Basin, Eastern Cordillera, and Middle Magdalena Valley, Colombia. American Association of Petroleum Geologists Bulletin 79, 1421–1443.

Dunham, R.J., 1962. Classification of carbonate rocks according to depositional texture. In: Hamm, W.E. (Ed.), Classification of Carbonate Rocks- A Symposium. American Association of Petroleum Geologists Bulletin, Special publication, Memoir 1, pp. 108–121.

Etayo, F., 1968. El sistema Cretáceo en la región de Villa de Leyva y zonas próximas. Geología Colombiana 5, 5–74.

Etayo, F., Renzoni, G., Barrero, D., 1976. Contornos sucesivos del mar Cretácico en Colombia. Primer Congreso Geológico Colombiano, Memoria 1 pp. 217–252 (Bogotá).

Fabre, A., 1983a. La subsidencia de la cuenca del Cocuy (Cordillera Oriental de Colombia) durante el cretáceo y el Terciario inferior. Primera parte: Estudio cuantitativo de la subsidencia. Geología Norandina 8, 49–61.

Fabre, A., 1983b. La subsidencia de la cuenca del Cocuy (Cordillera Oriental de Colombia) durante el cretáceo y el Terciario inferior. Segunda parte: Esquema de evolución tectónica. Geología Norandina 8, 21–27.

Fabre, A., Delaloye, M., 1983. Intrusiones básicas Cretácicas de la Cordillera Oriental. Geología Norandina 6, 19–28.

Forero, H., Sarmiento, G., 1985. La facies evaporítica de la Formación Paja en Villa en la región de Leyva, Chapter XVII. In: Etayo, F., Laverde-Montaño, F. (Eds.), Proyecto Cretácico, contribuciones. Publicaciones Geológicas Especiales Ingeominas 16, p. 16 Bogotá.

Galarraga, F., Reategui, K., Martínez, A., Martínez, M., Llamas, J.F., Márquez, G., 2008. V/Ni ratio as a parameter in palaeoenvironmental characterization of nonmature medium-crude oils from several Latin American basins. Journal of Petroleum Science and Engineering 61:9–14. https://doi.org/10.1016/j.petrol.2007.10.001.

Gaona-Narváez, T., Maurrasse, F.J., Etayo, F., 2013. Geochemistry, palaeoenvironments and timing of Aptian organic-rich beds of the Paja Formation (Curití, Eastern Cordillera, Colombia). In: Bojar, A.V., Melinte-Dobrinescu, M.C., Smit, J. (Eds.), Isotopic Studies in Cretaceous Research. Geological Society of London, Special Publication 382. https://doi.org/10.1144/SP382.6.

Goldberg, K., Humayun, M., 2016. Geochemical paleoredox indicators in organic-rich shales of the Irati Formation, Permian of the Paraná Basin, southern Brazil. Brazilian Journal of Geology 46 (3):377–393. https://doi.org/10.1590/2317-4889201620160001.

Guerrero, J., 2002. A proposal on the classification of systems tracts: application to the allostratigraphy and sequence stratigraphy of the Cretaceous Colombian Basin. Part 2: Barremian to Maastrichtian. Geología Colombiana 27, 27–49.

Guerrero, J., Sarmiento, G., Navarrete, R., 2000. The Stratigraphy of the W side of the Cretaceous Colombian Basin in the Upper Magdalena Valley. Reevaluation of selected areas and type localities including Aipe, Guaduas, Ortega and Piedras. Geología Colombiana 25, 45–104.

Hatch, J.R., Leventhal, J.S., 1992. Relationship between inferred redox potential of the depositional environment and geochemistry of the Upper Pennsylvanian (Missourian) stark shale member of the Dennis Limestone, Wabaunsee County, Kansas, USA. Chemical Geology 99, 65–82.

He, C., Ji, L., Wu, Y., Su, A., Zhang, M., 2016. Characteristics of hydrothermal sedimentation process in the Yanchang Formation, south Ordos Basin, China: evidence from element geochemistry. Sedimentary Geology 345, 33–41.

Jenkyns, H.C., 2010. Geochemistry of ocean anoxic events. Geochemistry, Geophysics, Geosystems 11, Q03004. https://doi.org/10.1029/2009GC002788.

Jones, B., Manning, D.A.C., 1994. Comparison of geochemical indices used for the interpretation of palaeoredox conditions in ancient mudstones. Chemical Geology 111, 111–129.

Ketzer, J.M., Morad, S., Amorosi, A., 2003. Predictive diagenetic clay-mineral distribution in siliciclastic rocks within a sequence stratigraphic framework. In: Worden, R.H., Morad, S. (Eds.), Clay Mineral Cements in Sandstones. International Association of Sedimentologists Special Publication 34, pp. 43–61.

Kietzmann, D.A., Palma, R.M., 2009. Tafofacies y biofacies de la Formación Vaca Muerta en el sector surmendocino de la Cuenca Neuquina: implicancias paleoecológicas, sedimentológicas y estratigráficas. Ameghiniana 46, 321–343.

Kietzmann, D.A., Palma, R.M., Bressan, G.S., 2008. Facies y microfacies de la rampa Thitoniana-Berriasiana de la Cuenca Neuquina (Formación Vaca Muerta) en la asociación del Arroyo Loncoche-Malargüe, provincia de Mendoza. Revista de la Asociación Geológica Argentina 63, 696–713.

Kietzmann, D.A., Palma, R.M., Riccardi, A.C., Martín-Chivelet, J., López-Gómez, J., 2014. Sedimentology and sequence Stratigraphy of a Tithonian-Valanginian carbonate ramp (Vaca Muerta Formation): a misunderstood exceptional source rock in the southern Mendoza area of Neuquén Basin, Argentina. Sedimentary Geology 302, 64–86.

Kietzmann, D.A., Ambrosio, A.L., Suriano, J., Alonso, M.S., Tomassini, F.G., Depine, G., Repol, D., 2016. The Vaca Muerta-Quintuco system (Tithonian-Valanginian) in the Neuquén Basin, Argentina: a view from the outcrops in the Chos Malal fold and thrust belt. American Association of Petroleum Geologists Bulletin 100, 743–771.

Macellari, C.E., De Vries, T.J., 1987. Late Cretaceous upwelling and Anoxic sedimentation in northwestern South America. Palaeogeography, Palaeoclimatology, Palaeoecology 59, 279–292.

Martini, R., Cirilli, S., Saurer, C., Abate, B., Ferruza, G., Lo Ciero, G., 2007. Depositional environment and biofacies characterization of the Triassic (Carnian to Rhaetian) carbonate succession of Punta Bassano (Marettimo Island, Sicily). Facies 53, 389–400.

McLaughlin, D., 1972. Evaporite deposits of Bogota area, Cordillera Oriental, Colombia. American Association of Petroleum Geologists Bulletin 56, 2240–2259.

McLennan, S.C., 2001. Relationship between the trace element composition of sedimentary rocks and upper continental crust. Geochemistry, Geophysics, Geosystems 2 (200GC000109). https://doi.org/10.1029/2000GC000109.

Meyer, K.M., Kump, L.R., 2008. Oceanic euxinia in earth history: causes and consequences. Annual Review of Earth and Planetary Sciences 36:251–288. https://doi.org/10.1146/annurev.earth.36.031207.124256.

Moreno, G., Sarmiento, G., 2002. Estratigrafía cuantitativa de las Formaciones Tablazo y Simití en las localidades de Sáchica (Boyacá) y Barichara-San Gil (Santander), Colombia. Geología Colombiana 27, 51–74.

Patarroyo, P., 2009. Amonitas de un nivel de alta energía del Barremiano inferior en la Formación Paja de los sectores de Villa de Leyva (Boyacá) y de Vélez (Santander). Boletín de Geología 31, 15–21.

Pemberton, S.G., MacEachern, J.A., 1997. The ichnological signature of storm deposits: the use of trace fossils in event stratigraphy. In: Brett, C.E. (Ed.), Paleontological Event Horizons-Ecological and Evolutionary Implications. Columbia University Press, New York, pp. 73–109.

Read, J.F., 1985. Carbonate platform facies models. American Association of Petroleum Geologists Bulletin 69, 1–21.

Rebesco, M., Hernández-Molina, F.J., Van Rooij, D., Wåhlin, A., 2014. Contourites and associated sediments controlled by deep-water circulation processes: state-of-the-art and future considerations. Marine Geology 352, 111–154.

Rimmer, S., 2004. Geochemical paleoredox indicators in Devonian-Mississippian black shales, Central Appalachian Basin (USA). Chemical Geology 206:373–391. https://doi.org/10.1016/j.chemgeo.2003.12.029.

Rivera, H.A., Sánchez, L.K., Suárez, N.S., Piragüa, A., 2016. Inorganic geochemistry as technique to preliminary assessment of shale plays in Cretaceous source rocks in the eastern Cordillera Basin, Colombia. American Association of Petroleum Geologists Annual Convention and Exhibition, Calgary, Canada (Search and Discovery Article #90259).

Rodrigues, N., Cobbold, P.R., LØseth, H., Ruffet, G., 2009. Widespread bedding-parallel veins of fibrous calcite ("beef") in a mature source rock (Vaca Muerta Fm., Neuquén basin, Argentina): evidence for overpressure and horizontal compression. Journal of the Geological Society of London 166, 695–709.

Sarmiento-Rojas, L.F., 2002. Condiciones geológicas favorables de las sedimentitas Cretácicas de la Cordillera Oriental de Colombia para la existencia de depósitos exhalativos submarinos de Plomo y Zinc. Boletín de Geología 24, 49–72.

Sarmiento-Rojas, L.F., 2011. Eastern Cordillera Basin, v. 7. In: Cediel, F., Ojeda, G., Colmenares, F. (Eds.), Petroleum Geology of Colombia. Fondo Editorial Universidad EAFIT, Medellín, Colombia, p. 140.

Sarmiento-Rojas, L.F., Van Wess, J.D., Cloetingh, S., 2006. Mesozoic transtensional basin history of the Eastern Cordillera, Colombian Andes: inferences from tectonic models. Journal of South American Earth Sciences 21, 383–411.

Shanmugam, G., 2008. Deep-water bottom currents and their deposits. In: Rebesco, M., Camerlenghi, A. (Eds.), Contourites. Developments in Sedimentology. vol. 60. Elsevier, Amsterdam, pp. 59–81.

Shanmugam, G., 2013. Modern internal waves and internal tides along oceanic pycnoclines: challenges and implications for ancient deep-marine baroclinic sands. American Association of Petroleum Geologists Bulletin 97, 767–811.

Spalletti, L.A., Franzese, J.R., Matheos, S.D., Schwarz, E., 2000. Sequence stratigraphy of a tidally dominated carbonate-siliciclastic ramp; the Tithonian–Early Berriasian of the Southern Neuquén Basin, Argentina. Geological Society of London, Special Publication 157, 433–446.

Spalletti, L.A., Poiré, D.G., Schwarz, E., Veiga, G.D., 2001. Sedimentological and sequence stratigraphic model of a Neocomian marine carbonate-siliciclastic ramp: Neuquén Basin, Argentina. Journal of South American Earth Sciences 14, 609–624.

Stow, D.A.V., Huc, A.Y., Bertrand, P., 2001. Depositional processes of black shales in deep water. Marine and Petroleum Geology 18, 491–498.

Taboada, A., Rivera, L.A., Fuenzalida, A., Cisternas, A., Philip, H., Bijawaard, H., Olaya, J., Rivera, C., 2000. Geodynamic of the northern Andes: subductions and intracontinental deformation (Colombia). Tectonics 19, 787–813.

Taylor, K.G., Machent, P.G., 2010. Systematic sequence-scale controls on carbonate cementation in a siliciclastic sedimentary basin: examples from Upper Cretaceous shallow marine deposits of Utah and Colorado, USA. Marine and Petroleum Geology 27, 1297–1310.

Taylor, K.G., Gawthorpe, R.L., Curtis, C.D., Marshall, J.D., Awwiller, D.N., 2000. Carbonate cementation in a sequence-stratigraphic framework: Upper Cretaceous sandstones, Book Cliffs, Utah-Colorado. Journal of Sedimentary Research 70, 360–372.

Terraza, R., 2012. Estratigrafía y ambientes de depósito de la Arenisca de Chiquinquirá en los alrededores de la localidad tipo. Boletín de Geología 34, 55–72.

Trabucho-Alexandre, J., Tuenter, E., Henstra, G.A., van der Zwan, K.J., van del Wal, R.S.W., Dijkstra, H.A., de Boer, P.L., 2010. The mid-Cretaceous North Atlantic nutrient trap: black shales and OAEs. Paleoceanography and Paleoclimatology 25, PA4201. https://doi.org/10.1029/2010PA001925.

Tribovillard, N.P., Stephan, J.F., Manivit, H., Reyre, Y., Cotillon, P., Jautée, E., 1991. Cretaceous black shales of Venezuelan Andes: preliminary results on stratigraphy and palaeoenvironmental interpretations. Palaeogeography, Palaeoclimatology, Palaeoecology 81, 313–321.

Tribovillard, N.P., Algeo, T.J., Lyons, T., Riboulleau, A., 2006. Trace metals as paleoredox and paleoproductivity proxies: an update. Chemical Geology 232:12–32. https://doi.org/10.1016/j.chemgeo.2006.02.012.

Tucker, M.E., Wright, V.P., 1990. Carbonate sedimentology. Blackwell Science Ltd., Oxford, p. 468.

Tyson, R.V., Pearson, T.H., 1991. Modern and ancient continental shelf anoxia: an overview. In: Tyson, R.V., Pearson, T.H. (Eds.), Modern and Ancient Continental Shelf Anoxia. Geological Society of London, Special Publication 58, pp. 1–24.

Villamil, T., 1993. Relative sea-level, chronology, and a new sequence stratigraphy model for a distal offshore facies, Albian to Santonian, Colombia. In: Pindell, J., Drake, C. (Eds.), Mesozoic-Cenozoic Stratigraphy and Tectonic Evolution of the Caribbean Region/Northern South America: Implications for Eustasy From Exposed Sections of the Cretaceous-Eocene Passive Margin Setting. C-8. Geological Society of America Memoir, paper.

Villamil, T., 1996. Paleobiology of two new species of the bivalve *Anomia* from Colombia and Venezuela and the importance of the genus in recognition of the base of Turonian. Cretaceous Research 17, 607–632.

Villamil, T., 1998. Chronology, relative sea-level history and new sequence stratigraphic model of basinal cretaceous facies of Colombia. In: Pindell, J., Drake, C. (Eds.), Paleogeographic evolution and non-Glacial Eustasy, Northern South America. Society for Sedimentary Geology, Special Publication 58, pp. 161–216.

Villamil, T., Arango, C., 1998. Integrated stratigraphy of latest Cenomanian and early Turonian facies of Colombia. In: Pindell, J., Drake, C. (Eds.), Paleogeographic Evolution and Non-Glacial Eustasy, Northern South America. Society for Sedimentary Geology, Special Publication 58, pp. 129–159.

Wedepohl, K.H., 1971. Environmental influences on the chemical composition of shales and clays. In: Ahrens, L.H., Press, F., Runcorn, S.K., Urey, H.C. (Eds.), Physics and Chemistry of the Earth. vol. 8. Pergamon, Oxford, pp. 307–331.

Wedepohl, K.H., 1991. The composition of the upper earth's crust and the natural cycles of selected metals. Metals in natural raw materials. Natural Resources. In: Merian, E. (Ed.), Metals and Their Compounds in the Environment. VCH, Weinheim, pp. 3–17.

Zecchin, M., Catuneanu, O., 2013. High-resolution sequence stratigraphy of clastic shelves I: units and bounding surfaces. Marine and Petroleum Geology 39:1–25. https://doi.org/10.1016/j.marpetgeo.2012.08.015.

Zecchin, M., Catuneanu, O., 2017. High-resolution sequence stratigraphy of clastic shelves VI: mixed siliciclastic-carbonate systems. Marine and Petroleum Geology 88: 712–723. https://doi.org/10.1016/j.marpetgeo.2017.09.012.